PERGAMON

International Journal of Solids and Structures 36 (1999) 2341–2378

INTERNATIONAL JOURNAL OF SOLIDS and STRUCTURES

A thermomechanical model for the analysis of light alloy solidification in a composite mould

Diego Celentano[a,*], Dayalan Gunasegaram[b], Thang Nguyen[b]

[a] *E.T.S. d'Enginyers de Camins, Canals i Ports, International Center for Numerical Methods in Engineering (CIMNE), Universitat Politènica de Catalunya, Gran Capità s/n, Mòdul C1, 08034 Barcelona, Spain*

[b] *The University of Queensland, CSIRO Division of Manufacturing Technology, CRC for Alloy and Solidification Technology (CAST), Locked Bag 9, Preston 3072, Australia*

Received 28 February 1997; in revised form 16 March 1998

Abstract

A coupled thermomechanical model to simulate light alloy solidification problems in permanent composite moulds is presented. This model is based on a general isotropic thermoelasto-plasticity theory and considers the different thermomechanical behaviours of each component of the mould as well as those of the solidifying material during its evolution from liquid to solid. To this end, plastic evolution equations, a phase-change variable and a specific free energy function are proposed in order to derive temperature-dependent material constitutive laws.

The corresponding finite element formulation and the staggered scheme used to solve the coupled non-linear system of equations are also presented. Finally, the temperature and displacement predictions of the model are validated with laboratory measurements obtained during an experimental trial.

Keywords: Casting process; Light alloy solidification; Permanent composite mould; Coupled thermomechanical analysis

1. Introduction

Several thermomechanical formulations for numerical modelling of different casting processes have been developed by many researchers during the last years (see e.g. Bellet et al., 1993, 1996; Celentano, 1994; Celentano et al., 1995, 1996; Chow et al., 1995; Gunasegaram et al., 1997; Heinlein et al., 1986; Smelser and Richmond, 1988; Trovant and Argyropoulos, 1996; Vicente-

* Corresponding author. Departamento de Ingeniería Mecánica, Universidad de Santiago de Chile, Avda. Bdo. O'Higgins 3363, Santiago de Chile, Chile. E-mail: dcelenta@lauca.usach.cl

0020–7683/99/$ - see front matter
PII: S0020–7683(98)00114–0

Hernandez et al., 1995; Williams et al., 1990; Zabaras et al., 1990; 1991; and references therein) in acknowledgement of the need to drive solidification modelling capabilities beyond traditional limits defined by purely thermal simulation tools.

The thermomechanical simulation of the light alloy solidification in a permanent composite mould is particularly complex due to, mainly, the phase-change effects, the different kind of mould materials usually considered and the variable thermomechanical contact conditions caused by gap formation occurring at the casting–mould interface. It is well known that the formation of this gap results in a substantial reduction in heat transfer rates across such interface and hence is an important factor in a solidification analysis (see e.g. Bellet et al., 1993, 1996; Celentano, 1994; Celentano et al., 1995; Gunasegaram et al., 1997; Smelser and Richmond, 1988; Trovant and Argyropoulos, 1996; Vicente-Hernandez et al., 1995).

This paper describes a coupled thermomechanical model for the analysis of light alloy solidification problems in permanent composite moulds. The general thermomechanical context is presented in Section 2 while Section 3 includes the constitutive models, formulated in the plasticity theory framework, assumed for the materials involved in the process. In particular, the main new features of the light alloy model proposed in this work are the consideration of an experimental-based phase-change function, a temperature-dependent specific latent heat value and a phase-change strain tensor in the constitutive laws, the choice of the internal variables with their evolution equations accounting for the material state (liquid, mushy or solid) and a clear definition of the difference between tangent and secant thermomechanical material properties used in the model definition. Moreover, the expressions for all the constitutive laws of this original model are also presented.

Further, the corresponding finite element formulation and the numerical strategy adopted to solve the highly non-linear discretized equations are described in Section 4 and 5, respectively. Finally, Section 6 contains the simulation of two simple casting examples and an experimental validation of this model considering a light alloy solidification test.

2. Thermomechanical formulation

Let some open bounded domains $\Omega_{(i)} \subset \mathbb{R}^{n}_{\text{dim}}$ ($1 \leqslant n_{\text{dim}} \leqslant 3$ and $i = 1, \ldots, n_{\text{body}}$) be the reference (initial) configurations of some n_{body} continuum thermoelasto-plastic bodies $\mathscr{B}_{(i)}$ (that may thermomechanically interact between themselves) with material coordinates labeled by $\boldsymbol{X} \in \Omega_{(i)}$ (all of them measured with respect to the same reference coordinate system), $\Gamma_{(i)} = \partial\Omega_{(i)}$ their smooth boundaries, respectively, and $\Upsilon \subset \mathbb{R}^{+}$ be the time interval of analysis ($t \in \Upsilon$). Typically, subindex (i) is used to identify the alloy and the different parts (often of different materials) composing the mould. For simplicity in the notation, subscript (i) will be dropped from here onwards. Moreover, infinitesimal displacements/strain relationships are assumed.

In the context of general thermodynamics (see e.g. Coleman and Gurtin, 1967; Lubliner, 1990; Ziegler 1969), the existence of the specific Helmholtz free energy function $\psi = \hat{\psi}(\boldsymbol{\varepsilon}, \boldsymbol{\alpha}_k, T) = \omega - \eta T$ can be assumed as a function of the thermodynamic state variables $\boldsymbol{\varepsilon}$, $\boldsymbol{\alpha}_k$ and T, where $\boldsymbol{\varepsilon}$ is the strain tensor (in tensor notation, $\boldsymbol{\varepsilon} = 1/2\ (\boldsymbol{\nabla} \otimes \boldsymbol{u} + \boldsymbol{u} \otimes \boldsymbol{\nabla})$, where $\boldsymbol{u}$ is the displacement vector and $\boldsymbol{\nabla} = \partial/\partial \boldsymbol{X}$ is the gradient operator), $\boldsymbol{\alpha}_k$ is the n_{int}-dimensional ($k = 1, \ldots, n_{\text{int}}; n_{\text{int}} \geqslant 1$) vector field of phenomenological internal state variables (usually governed by rate equations with their cor-

responding initial conditions) and T is the temperature. Moreover, ω is the specific internal energy and η is the specific entropy. The consideration of the Coleman method leads to the following relations (see e.g. Coleman and Gurtin, 1967): $\boldsymbol{\sigma} = \rho_0 \partial\psi/\partial\boldsymbol{\varepsilon}$ and $\eta = -\partial\psi/\partial T$, such that $\boldsymbol{\sigma}$ is the stress tensor and ρ_0 is the density at the initial configuration. As a consequence of these equations, $\omega = \psi - \partial\psi/\partial T T$. Therefore, the governing local equations describing a general thermomechanical process can be written in this framework as:

—equation of motion,

$$\boldsymbol{\nabla}\cdot\boldsymbol{\sigma} + \rho_0 \boldsymbol{b}_F = \rho_0 \ddot{\boldsymbol{u}} \quad \text{in } \Omega \times \Upsilon, \tag{2.1}$$

—heat balance equation,

$$-\rho_0 c \dot{T} - \boldsymbol{\nabla}\cdot\boldsymbol{q} + \rho_0 r - T\boldsymbol{\beta}:\dot{\boldsymbol{\varepsilon}} + \rho_0 r_{\text{int}} = 0 \quad \text{in } \Omega \times \Upsilon, \tag{2.2}$$

—dissipation equation,

$$-\boldsymbol{q}\cdot\boldsymbol{\nabla}T + D_{\text{int}} \geqslant 0 \quad \text{in } \Omega \times \Upsilon, \tag{2.3}$$

together with appropriate boundary and initial conditions and the following additional constitutive equations: $c = -T\partial^2\psi/\partial T^2$ is the tangent specific heat capacity, $\boldsymbol{q} = -\boldsymbol{k}\cdot\boldsymbol{\nabla}T$ is the heat flux vector defined according to the Fourier law ($\boldsymbol{k}$ being the conductivity tensor), $\boldsymbol{\beta} = -\rho_0 \partial^2\psi/\partial\boldsymbol{\varepsilon}\,\partial T = -\partial\boldsymbol{\sigma}/\partial T$ is the tangent conjugate of the thermal dilatation tensor and $r_{\text{int}} = (T\partial^2\psi/\partial\boldsymbol{\alpha}_k\,\partial T - \partial\psi/\partial\boldsymbol{\alpha}_k) \odot \dot{\boldsymbol{\alpha}}_k$ is the specific internal heat source. Furthermore, $\boldsymbol{b}_F$ is the specific body force, r is the specific heat source, the superposed dot denotes time derivative and the symbol $\odot$ indicates the appropriate multiplication conforming to the nature of each internal variable $\boldsymbol{\alpha}_k$. In eqn (2.3), $D^{th} = -\boldsymbol{q}\cdot\boldsymbol{\nabla}T$ and $D_{\text{int}} = \boldsymbol{q}_k \odot \dot{\boldsymbol{\alpha}}_k$ are the so-called thermal and internal dissipations, respectively, where $\boldsymbol{q}_k = \boldsymbol{q}_k(\boldsymbol{\varepsilon}, \boldsymbol{\alpha}_k, T) = -\rho_0 \partial\psi/\partial\boldsymbol{\alpha}_k$ are clearly the conjugate variables of $\boldsymbol{\alpha}_k$. Instead of eqn (2.3), an additional more restrictive dissipative assumption is to consider $D^{th} \geqslant 0$ and $D_{\text{int}} \geqslant 0$ (see e.g. Coleman and Gurtin, 1967). In such a case, the first condition is automatically fulfilled if $|\boldsymbol{k}| \geqslant 0$ ($|\,|$ is the determinant symbol) where, for the particular case of isotropic conduction $\boldsymbol{k} = k\mathbf{1}$ (k being the conductivity coefficient and $\mathbf{1}$ the unity tensor), it leads to $k \geqslant 0$.

As it can be seen, the definition of ψ constitutes a crucial point of the formulation since it is the basis for the derivation of all the constitutive equations to be described in Section 3.

Although the boundary conditions have not been explicitly stated here (a full description of them can be found in Celentano et al., 1996), they will be discussed in the thermomechanical finite element formulation of Section 4.

3. Constitutive models

3.1. Internal variables

With the sake of describing the behaviour of the materials involved in the light alloy solidification in a composite mould, the following split is proposed: $n_{\text{int}} = n^p_{\text{int}} + n^{pc}_{\text{int}}$, where n^p_{int} and n^{pc}_{int} denote the number of internal variables related to plastic (non-reversible and assumed to occur in every material existing in the process) and phase-change effects (only experience by the alloy), respectively. Accordingly, $r_{\text{int}} = r^p_{\text{int}} + r^{pc}_{\text{int}}$ and $D_{\text{int}} = D^p_{\text{int}} + D^{pc}_{\text{int}}$. Further, a more simpler model takes

place if the same n_{int}^p intern variables are defined for both the components of the mould and the light alloy.

In the context of the rate-independent plasticity theory (see e.g. Lubliner, 1990), the thermoplastic behaviour of the solid is governed by a yield function $F = \hat{F}(\boldsymbol{\varepsilon}, \boldsymbol{\alpha}_k, T)$; $k = 1, \ldots, n_{\text{int}}^p$ (assumed strictly convex and, for simplicity, defined in terms of a unique smooth function) such that no plastic evolutions occur when $F < 0$.

Further, the assumption of the principle of maximum plastic dissipation together with the load–unload Kuhn–Tucker conditions and the Prager's consistency condition, leads to an associate temperature-dependent constitutive model characterized by plastic evolution equations of the type $\dot{\boldsymbol{\alpha}}_k = \dot{\lambda}\boldsymbol{g}_k$ in addition with some conditions over $\boldsymbol{q}_k$, F and $\boldsymbol{g}_k$, where $\dot{\lambda}$ is the plastic consistency parameter and $\boldsymbol{g}_k$ are known functions (see e.g. Armero and Simo, 1992b; Celentano et al., 1996; Lubliner, 1990). In this paper, the following possible option has been chosen for such equations: $(\boldsymbol{\alpha}_1 = \boldsymbol{\varepsilon}^p,\ \alpha_2 = \vartheta^p,\ \boldsymbol{\alpha}_3 = \boldsymbol{\kappa}^p,\ \alpha_4 = \zeta^p;\ n_{\text{int}}^p = 4)$ and $(\boldsymbol{q}_1 = \boldsymbol{\sigma},\ q_2 = \mathscr{C}^p,\ \boldsymbol{q}_3 = \mathscr{K}^p,\ q_4 = T)$ with $F = \hat{F}(\boldsymbol{\sigma}, \mathscr{C}^p, \mathscr{K}^p, T)$, where $\boldsymbol{\varepsilon}^p$ is the plastic strain tensor, ϑ^p is the plastic isotropic hardening variable, $\boldsymbol{\kappa}^p$ is the plastic kinematic hardening tensor, ζ^p is a plastic 'yield' entropy, $\mathscr{C}^p$ is the plastic isotropic hardening function and $\mathscr{K}^p$ is the so-called back stress tensor, with the following evolution equations:

$$\dot{\boldsymbol{\varepsilon}}^p = \dot{\lambda}\frac{\partial F}{\partial \boldsymbol{\sigma}}, \tag{3.1}$$

$$\dot{\vartheta}^p = \dot{\lambda} H_\vartheta \frac{\partial F}{\partial \mathscr{C}^p}, \tag{3.2}$$

$$\dot{\boldsymbol{\kappa}}^p = \dot{\lambda}\, H_\kappa \frac{\partial F}{\partial \mathscr{K}^p}, \tag{3.3}$$

$$\dot{\zeta}^p = \dot{\lambda}\frac{\partial F}{\partial T}, \tag{3.4}$$

where H_ϑ is a function accounting for the isotropic strain or work hardening behaviours while H_κ is a function related to the kinematic hardening behaviour. In eqns (3.1)–(3.4), $(\boldsymbol{g}_1 = \partial F/\partial \boldsymbol{\sigma}, g_2 = H_\vartheta\, \partial F/\partial \mathscr{C}^p, \boldsymbol{g}_3 = H_\kappa\, \partial F/\partial \mathscr{K}^p, g_4 = \partial F/\partial T)$ where $\boldsymbol{R} = \partial F/\partial \boldsymbol{\sigma}$ is normally known as the flow potential tensor. Note that the evolution equation for ζ^p is consistent with the principle of maximum plastic dissipation in this thermomechanical context. Besides, zero initial conditions are considered for eqns (3.1)–(3.4). The expression for the yield function will be given below.

The phase-change in the alloy is taken into account by means of the liquid–solid phase-change function $f_{pc} \in [0, 1]$ (see e.g. Celentano et al., 1994; Celentano and Pérez, 1996) $(\alpha_5 = f_{pc}; n_{\text{int}}^{pc} = 1)$ such that, $f_{pc} = 1$ in the liquid phase and $f_{pc} = 0$ in the solid phase. Note that, in order to obtain a unified definition of the constitutive models, the condition $f_{pc} = 0$ is assumed for the mould components. In general, the evolution of f_{pc} in the mushy zone comes from a microstructural model (see e.g. Thévoz et al., 1989). However, a simplified model is achieved by considering that f_{pc} depends explicitly on T. In this particular case, the tangent specific heat capacity is now given by (see e.g. Celentano et al., 1996):

$$c = -T\frac{\partial^2\psi}{\partial T^2} - L\frac{\partial f_{pc}}{\partial T} \tag{3.5}$$

where $L = \hat{L}(T)$ is the tangent specific latent heat and, furthermore, the internal dissipation term due to the evolution of $f_{pc} = \hat{f}_{pc}(T)$, i.e. $D^{pc}_{\text{int}} = -\rho_0\,\partial\psi/\partial f_{pc}\dot{f}_{pc}$, is implicitly included in the definition of the entropy given in Section 2. Therefore, it can be demonstrated that r^{pc}_{int} and D^{pc}_{int} should not be considered in eqns (2.2) and (2.3), respectively. Within this context, the phase-change occurs in a range of temperatures $(T_l - T_s)$, where T_s and T_l are the solidus and liquidus temperatures of the alloy respectively, such that:

$$f_{pc} = \begin{cases} 0 & ;\forall T < T_s \\ 0 \leqslant g_{pc} \leqslant 1 & ;T_s \leqslant \forall T \leqslant T_l, \\ 1 & ;\forall T > T_l \end{cases} \tag{3.6}$$

where the function $g_{pc} = \hat{g}_{pc}(T)$ may be obtained from experimental observations (see e.g. Celentano and Pérez, 1996; Gunasegaram et al., 1997).

With these considerations, a Von Mises isotropic temperature-dependent yield function has been adopted:

$$F = \sqrt{3J_{2_\kappa}} - \mathscr{C}, \tag{3.7}$$

where $J_{2_\kappa} = 1/2[\boldsymbol{\sigma} - (1-f_{pc})\mathscr{K}^p]' : [\boldsymbol{\sigma} - (1-f_{pc})\mathscr{K}^p]'$ is the second invariant of the deviatoric tensor $\boldsymbol{\sigma}' - (1-f_{pc})\mathscr{K}^{p\prime}$ and $\mathscr{C} = \hat{\mathscr{C}}(\mathscr{C}^p, T)$ is the total hardening function defined by:

$$\mathscr{C} = \mathscr{C}^{th} + (1-f_{pc})\mathscr{C}^p, \tag{3.8}$$

where $\mathscr{C}^{th} = \hat{\mathscr{C}}^{th}(T)$ is the thermal hardening function (assumed to be a smooth function of T). Clearly, $\mathscr{C}^{th}$ is the temperature-dependent yield stress such that $\mathscr{C}^{th} \to 0$ in the liquid phase. Moreover, the derivatives of F appearing in eqns (3.1)–(3.4) are $\boldsymbol{R} = \sqrt{3}/(2\sqrt{J_{2_\kappa}})(\boldsymbol{\sigma} - \mathscr{K}^p)'$, $\partial F/\partial \mathscr{C}^p = -(1-f_{pc})$, $\partial F/\partial T = -\partial \mathscr{C}^{th}/\partial T + \partial f_{pc}/\partial T \mathscr{C}^p$ and $\partial F/\partial \mathscr{K}^p = -(1-f_{pc})\boldsymbol{R}$, respectively. Definitions (3.7) and (3.8) are based on the assumption that the plastic behaviour of the material is only due to its solid fraction expressed by $(1-f_{pc})$. At this stage, three important remarks may be drawn: (1) classical plastic evolution equations are recovered for the solid phase ($f_{pc} = 0$), (2) no hardening effects occur in the liquid phase ($f_{pc} = 1$) and (3) the mushy zone ($0 < f_{pc} < 1$) is described by weighting through the factor $(1-f_{pc})$ the former two limiting situations.

In this context, $H_\vartheta = -1$ or $H_\vartheta = -[\boldsymbol{\sigma} - (1-f_{pc})\mathscr{K}^p] : \boldsymbol{R}$ for the isotropic strain or work hardening cases, respectively, while the simple Melan–Prager model (i.e., $H_\kappa = 1$) is assumed [in a general case, however, H_κ could be a tensor representing, for instance, the 'fading strain memory' effect (see e.g. Lubliner, 1990)].

3.2. Specific free energy function

Restricting the analysis to the case of thermoelastic–plastic isotropic response, the following specific free energy function $\psi = \hat{\psi}(\boldsymbol{\varepsilon}, \boldsymbol{\varepsilon}^p, \vartheta^p, \boldsymbol{\kappa}^p, \zeta^p, T)$ is proposed:

$$\psi = \psi_{te} + \psi_{tp} + \psi_{pc}, \tag{3.9}$$

where $\psi_{te} = \hat{\psi}_{te}(\boldsymbol{\varepsilon}-\boldsymbol{\varepsilon}^p, T)$, $\psi_{tp} = \hat{\psi}_{tp}(\vartheta^p, \boldsymbol{\kappa}^p, \zeta^p, T)$ and $\psi_{pc} = \hat{\psi}_{pc}(\boldsymbol{\varepsilon}-\boldsymbol{\varepsilon}^p, T)$ are the thermoelastic, thermoplastic and phase-change parts of ψ, respectively. It should be noted that eqn (3.9) is a partially decoupled form of defining the specific free energy ψ. Considering that the decomposition of ψ into ψ_{te} and ψ_{tp} can nowadays be considered well established (see Armero and Simo, 1992b; see Kleiber, 1991; Lubliner, 1990), the adding of ψ_{pc}, firstly proposed by Celentano et al. (1996) for a simpler model than the one presented here, is an assumption based on the fact that phase-change effects are mainly governed by temperature. Once more, this definition is valid for both the components of the mould and the alloy in its different states (liquid, mushy and solid). In all the equations described below, the subscript 0 denotes the initial state of the different variables, while the superscript s indicates secant thermomechanical properties measured with respect to the reference temperature T_{ref} (e.g., the laboratory temperature). Additionally, $\boldsymbol{\varepsilon}_0 = \mathbf{0}$ is assumed.

The thermoelastic part ψ_{te} is written as:

$$\psi_{te} = \frac{1}{2\rho_0}(\boldsymbol{\varepsilon}-\boldsymbol{\varepsilon}^p)\colon \mathbb{C}^s\colon(\boldsymbol{\varepsilon}-\boldsymbol{\varepsilon}^p) - \frac{1}{\rho_0}(\boldsymbol{\varepsilon}-\boldsymbol{\varepsilon}^p)\colon \mathbb{C}^s\colon \boldsymbol{\varepsilon}^{th} + \psi_c - \psi_{c_0} + \frac{1}{\rho_0}(\boldsymbol{\varepsilon}-\boldsymbol{\varepsilon}^p)\colon \boldsymbol{\sigma}_0 - \eta_0(T-T_0) + \psi_0, \quad (3.10)$$

where $\mathbb{C}^s = \hat{\mathbb{C}}^s(T)$ is the secant elastic isotropic constitutive tensor and $\boldsymbol{\varepsilon}^{th} = \hat{\boldsymbol{\varepsilon}}^{th}(T)$ is the thermal strain tensor given by:

$$\boldsymbol{\varepsilon}^{th} = [\alpha^s_{th}(T-T_{\text{ref}}) - \alpha^s_{th_0}(T_0-T_{\text{ref}})]\mathbf{1}, \quad (3.11)$$

with $\alpha^s_{th} = \hat{\alpha}^s_{th}(T)$ being the secant thermal dilatation coefficient. Further, the function $\psi_c = \hat{\psi}_c(T)$ is:

$$\psi_c = -\int_{T_{\text{ref}}}^{T} A_c \, \mathrm{d}\theta, \quad (3.12)$$

where the function A_c is:

$$A_c = \int_{T_{\text{ref}}}^{T} \left[\frac{c^s}{\theta} + \frac{\partial c^s}{\partial \theta}\frac{(\theta - T_{\text{ref}})}{\theta}\right]\mathrm{d}\theta, \quad (3.13)$$

such that $c^s = \hat{c}^s(T)$ is the secant specific heat capacity. It should be noted that for the particular case of constant c^s, the more classical expression of ψ_c is obtained, i.e., $\psi_c\,|_{c^s = cte} = c^s(T-T_{\text{ref}}) - c^s T \ln T/T_{\text{ref}}$ (see e.g. Ziegler, 1983).

Although several sophisticated models considering more general hardening behaviours have been developed to better represent different material phenomena, a relatively simple form of writing the thermoplastic part of ψ is:

$$\psi_{tp} = -\frac{1}{2\rho_0}h_{\mathscr{C}^p}(\vartheta^p)^2 + \frac{1}{2\rho_0}h_{\mathscr{K}^p}\boldsymbol{\kappa}^p\colon \quad \boldsymbol{\kappa}^p - \frac{1}{\rho_0}T\zeta^p, \quad (3.14)$$

where $h_{\mathscr{C}^p} = \hat{h}_{\mathscr{C}^p}(T)$ and $h_{\mathscr{K}^p} = \hat{h}_{\mathscr{K}^p}(T)$ are the plastic isotropic and kinematic hardening moduli, respectively.

The phase-change part is:

$$\psi_{pc} = \psi_L - \psi_{L_0} - \frac{1}{\rho_0}(\boldsymbol{\varepsilon} - \boldsymbol{\varepsilon}^p) : \mathbb{C}^s : \boldsymbol{\varepsilon}^{pc}, \tag{3.15}$$

where the function $\psi_L = \hat{\psi}_L(T)$ is:

$$\psi_L = -\int_{T_{\text{ref}}}^{T} A_{pc}\, \mathrm{d}\theta, \tag{3.16}$$

with

$$A_{pc} = \int_{T_{\text{ref}}}^{T} \left[\frac{L^s}{\theta} \frac{\partial f_{pc}}{\partial \theta} + \frac{\partial L^s}{\partial \theta} \frac{(f_{pc} - f_{pc_{\text{ref}}})}{\theta} \right] \mathrm{d}\theta, \tag{3.17}$$

where $L^s = \hat{L}^s(T)$ is the secant specific latent heat, $f_{pc_{\text{ref}}}$ is the phase-change function at the reference temperature and $\boldsymbol{\varepsilon}^{pc} = \hat{\boldsymbol{\varepsilon}}^{pc}(T)$ is the phase-change strain tensor defined as:

$$\boldsymbol{\varepsilon}^{pc} = -\tfrac{1}{3}[\delta^s_{pc}(f_{pc} - f_{pc_{\text{ref}}}) - \delta^s_{pc_0}(f_{pc_0} - f_{pc_{\text{ref}}})]\mathbf{1}, \tag{3.18}$$

where $\delta^s_{pc} = \hat{\delta}^s_{pc}(T)$ is the secant phase-change volumetric deformation. The existence of this volumetric deformation is a well-known experimental fact in the solidification of many alloys (see Flemings et al., 1974). In sharp contrast with the present approach, this effect has been usually taken into account in several thermomechanical models by assuming a large variation of the thermal dilatation coefficient in the mushy zone (see e.g. Chow et al., 1995; Celentano et al., 1995).

A particular definition of $\mathbb{C}^s$ accounting for phase-change effects is considered in eqns (3.10) and (3.15) (see Celentano, 1996). During solidification, the alloy in liquid state becomes solid and, therefore, a qualitative change in its thermomechanical properties is produced. This fact is taken into account in the constitutive tensor written as:

$$\mathbb{C}^s = \mathbb{C}^s_{\text{vol}} + (1 - f_{pc})\mathbb{C}^s_{\text{dev}}, \tag{3.19}$$

where $\mathbb{C}^s_{\text{vol}}$ and $\mathbb{C}^s_{\text{dev}}$ are the volumetric and deviatoric parts of $\mathbb{C}^s$, respectively. Note that eqn (3.19) is an additional constitutive assumption implicitly contained in the proposed specific free energy function given above. The importance of this definition of $\mathbb{C}^s$ will be pointed out below.

With the present definition of ψ, expressed in terms of secant thermomechanical properties, the constitutive laws and the internal plastic dissipation can be obtained. Details of such derivations are given below.

3.3. Constitutive laws

According to the definition given in Section 2, the secant stress–strain constitutive law is:

$$\boldsymbol{\sigma} = \mathbb{C}^s : (\boldsymbol{\varepsilon} - \boldsymbol{\varepsilon}^p - \boldsymbol{\varepsilon}^{th} - \boldsymbol{\varepsilon}^{pc}) + \boldsymbol{\sigma}_0, \tag{3.20}$$

such that the additive strain decomposition is recovered as $\boldsymbol{\varepsilon}^e = \boldsymbol{\varepsilon} - \boldsymbol{\varepsilon}^p - \boldsymbol{\varepsilon}^{th} - \boldsymbol{\varepsilon}^{pc}$, where $\boldsymbol{\varepsilon}^e$ is the so-called elastic strain tensor. It should be noted that this secant or hyperelastic constitutive law circumvents the usual thermodynamic constraints (see Cassenti and Annigeri, 1989), depends exclusively on the thermoelastic and phase-change parts of the free energy function and is assumed to be valid for the material in its different states. In particular, taking into account the definition

of $\mathbb{C}^s$ and the secant constitutive relation given above [eqns (3.19) and (3.20), respectively], both the classical constitutive law of a liquid at rest (i.e., zero deviatoric stress) and that corresponding to a solid can be represented. It should be also noted that $\boldsymbol{R}$ is indeterminate when $\boldsymbol{\sigma}' = \mathbf{0}$ and $f_{pc} = 1$. However, as $\mathscr{C}^{th} > 0$ is assumed, it can be observed that $F < 0$ for this particular situation. Therefore, a purely elastic behaviour of the material ($\dot{\lambda} = 0$) is considered for this case.

Further, the definition of ψ given above allows to compute the conjugate of the internal plastic variables. It should be noted that the relations $\boldsymbol{\sigma} = -\rho_0 \partial\psi/\partial\boldsymbol{\varepsilon}^p$ and $T = -\rho_0 \partial\psi/\partial\zeta^p$ and fulfilled while $\mathscr{C}^p$ and $\mathscr{K}^p$ can be expressed by:

$$\mathscr{C}^p = h_{\mathscr{C}^p}\vartheta^p, \tag{3.21}$$

$$\mathscr{K}^p = -h_{\mathscr{K}^p}\boldsymbol{\kappa}^p, \tag{3.22}$$

resulting linear relations due to the particular definition of ψ^{tp} given by eqn (3.14).

The proposed expression for ψ allows us to derive the tangent variables of the model. Firstly, it is important to remark that $\mathbb{C} = \mathbb{C}^s$ ($\mathbb{C}$ being the tangent elastic constitutive tensor given by $\mathbb{C} = \partial\boldsymbol{\sigma}/\partial\boldsymbol{\varepsilon}$) due to the small displacements/strains context assumed here.

Considering eqn (3.20) and the definitions given in Section 2, the tangent conjugate of the thermal dilatation $\boldsymbol{\beta}$ appearing in eqn (2.2) is:

$$\boldsymbol{\beta} = \mathbb{C}^s : \left\{ \alpha^s_{th} + \frac{\partial \alpha^s_{th}}{\partial T}(T - T_{\text{ref}}) - \frac{1}{3}\left[\delta^s_{pc}\frac{\partial f_{pc}}{\partial T} + \frac{\partial \delta^s_{pc}}{\partial T}(f_{pc} - f_{pc_{\text{ref}}}) \right] \right\} \mathbf{1} + \frac{\partial \mathbb{C}^s}{\partial T} : \boldsymbol{\varepsilon}^e, \tag{3.23}$$

where for constant material properties and $\delta^s_{pc} = 0$ the standard expression is obtained, i.e., $\boldsymbol{\beta} \mid \mathbb{C}^s = cte$, $\alpha^s_{th} = cte$, $\delta^s_{pc} = 0 = \mathbb{C}^s : \alpha^s_{th}\mathbf{1}$. Tensor $\boldsymbol{\beta}$ can also be written as:

$$\boldsymbol{\beta} = \mathbb{C}^s : \left(\alpha_{th} - \frac{1}{3}\delta_{pc}\frac{\partial f_{pc}}{\partial T} \right) \mathbf{1} + \frac{\partial \mathbb{C}^s}{\partial T} : \boldsymbol{\varepsilon}^e, \tag{3.24}$$

where $\alpha_{th} = \alpha^s_{th} + \partial\alpha^s_{th}/\partial T(T - T_{\text{ref}})$ is the tangent thermal dilatation coefficient and $\delta_{pc} = \delta^s_{pc} + \partial\delta^s_{pc}/\partial T(f_{pc} - f_{pc_{\text{ref}}})(\partial f_{pc}/\partial T)^{-1}$ is the tangent phase-change volumetric deformation such that $\dot{\boldsymbol{\varepsilon}}^{th} = \alpha_{th}\mathbf{1}\dot{T}$ and $\dot{\boldsymbol{\varepsilon}}^{pc} = -1/3\delta_{pc}\mathbf{1}\dot{f}_{pc}$. The thermal and phase-change strain rates have been extensively used in the context of hypoelastic models to simulate casting processes (see e.g. Bellet et al., 1993, Chow et al., 1995; Smelser and Richmond, 1988; Zabaras et al., 1993, 1996). Moreover, defining the tangent specific latent heat L appearing in eqn (3.5) as:

$$L = L^s + \frac{\partial L^s}{\partial T}(f_{pc} - f_{pc_{\text{ref}}}) \left(\frac{\partial f_{pc}}{\partial T} \right)^{-1}, \tag{3.25}$$

the function A_{pc} can also be written in terms of L as:

$$A_{pc} = \int_{T_{\text{ref}}}^{T} \frac{L}{\theta}\frac{\partial f_{pc}}{\partial \theta}\,\mathrm{d}\theta. \tag{3.26}$$

It should be noted that for constant α^s_{th}, δ^s_{pc} and L^s, the respective tangent values coincide with these secant ones.

Using standard concepts of plasticity theory, the tangent constitutive law can be written as:

$$\dot{\boldsymbol{\sigma}} = \mathbb{C}^{ep}: \dot{\boldsymbol{\varepsilon}} - \boldsymbol{\beta}^{ep}\dot{T}, \tag{3.27}$$

where the elasto-plastic tangent constitutive tensor $\mathbb{C}^{ep}$ is:

$$\mathbb{C}^{ep} = \mathbb{C}^{s} - H(\dot{\lambda})\mathbb{C}^{s}: \boldsymbol{R} \otimes \boldsymbol{\Phi}, \tag{3.28}$$

and the thermoelasto-plastic tangent constitutive tensor $\boldsymbol{\beta}^{ep}$ is:

$$\boldsymbol{\beta}^{ep} = \boldsymbol{\beta} - H(\dot{\lambda})\chi\mathbb{C}^{s}: \boldsymbol{R}, \tag{3.29}$$

such that the plastic consistency parameter is given by:

$$\dot{\lambda} = \langle \boldsymbol{\Phi}: \dot{\boldsymbol{\varepsilon}} + \chi\dot{T} \rangle, \tag{3.30}$$

considering the following respective expressions for $\boldsymbol{\Phi}$ and χ:

$$\boldsymbol{\Phi} = \frac{1}{A_{\lambda}}\boldsymbol{R}: \mathbb{C}^{s}, \tag{3.31a}$$

$$\chi = \frac{1}{A_{\lambda}}(\boldsymbol{\beta}: \boldsymbol{R} + A_{\chi}), \tag{3.31b}$$

with

$$A_{\lambda} = \boldsymbol{R}: \mathbb{C}^{s}: \boldsymbol{R} - (1 - f_{pc})^{2}(h_{\mathscr{C}^{p}}H_{\vartheta} - h_{\mathscr{K}^{p}}H_{\kappa}\boldsymbol{R}: \boldsymbol{R}), \tag{3.31c}$$

$$A_{\chi} = (1 - f_{pc})\left(\frac{\partial h_{\mathscr{C}^{p}}}{\partial T}\vartheta^{p} - \frac{\partial h_{\mathscr{K}^{p}}}{\partial T}\boldsymbol{\kappa}^{p}: \boldsymbol{R}\right) + \frac{\partial \mathscr{C}^{th}}{\partial T} - \frac{\partial f_{pc}}{\partial T}\mathscr{C}^{p}, \tag{3.31d}$$

H being the Heaviside function and $\langle\ \rangle$ the Macauley symbol.

Furthermore, the well-known plastic restriction (see e.g. Lubliner, 1990) $\partial F/\partial \boldsymbol{\alpha}_k \odot \boldsymbol{g}_k < 0$ for $F = \dot{F} = 0$ reads for this constitutive model as $A_{\lambda} > 0$ for $F = \dot{F} = 0$ which is clearly satisfied if the additional constraint $(1 - f_{pc})^{2}(h_{\mathscr{C}^{p}}H_{\vartheta} - h_{\mathscr{K}^{p}}H_{\kappa}\boldsymbol{R}:\boldsymbol{R}) < \boldsymbol{R}: \mathbb{C}^{s}: \boldsymbol{R}$ is assumed, where $\boldsymbol{R}: \boldsymbol{R} = 3/2$ and the condition $\boldsymbol{R}: \mathbb{C}^{s}: \boldsymbol{R} > 0$ is verified taking into account the definitions given above. In the solid phase ($f_{pc} = 0$), the particular situation represented by $h_{\mathscr{C}^{p}}H_{\vartheta} - h_{\mathscr{K}^{p}}H_{\kappa}\boldsymbol{R}:\boldsymbol{R} < 0$ is characteristic of (strain or work) hardening plastic materials.

According to the definitions given above, the expressions of the specific entropy function $\eta = \hat{\eta}(\boldsymbol{\varepsilon} - \boldsymbol{\varepsilon}^{p}, \vartheta^{p}, \boldsymbol{\kappa}^{p}, \zeta^{p}, T)$, the specific internal energy $\omega = \hat{\omega}(\boldsymbol{\varepsilon} - \boldsymbol{\varepsilon}^{p}, \vartheta^{p}, \boldsymbol{\kappa}^{p}, \zeta^{p}, T)$ and the tangent specific heat capacity $c = \hat{c}(\boldsymbol{\varepsilon} - \boldsymbol{\varepsilon}^{p}, \vartheta^{p}, \boldsymbol{\kappa}^{p}, T)$ can be found in Box 1. It should be noted that they preserve the additive decomposition previously assumed for ψ.

It can be clearly observed that eqn (3.5) includes the classical definition of the specific heat capacity in the whole domain because the phase-change part of ψ does not play any role in the expression of c. In the particular case of constant properties, $c \mid_{\mathbb{C}^{s} = cte, \alpha^{s}_{th} = cte, c^{s} = cte} = c^{s}$ is obtained. Further, considering that $\boldsymbol{\varepsilon} - \boldsymbol{\varepsilon}^{p}$ is the thermoelastic deformation term (in the free energy definition sense), it should be noted that the instantaneous elasticity assumption of the specific heat capacity, usually accepted for metals (see e.g. Lubliner, 1990), is only fulfilled if the thermoplastic contribution c^{tp} is neglected (Gunasegaram et al., 1997; Heinlein et al., 1986).

The specific internal plastic heat source r^{p}_{int} is also described in Box 1 by means of two equivalent expressions.

Box 1
Specific entropy function, specific internal energy, tangent specific heat capacity and specific internal plastic heat source

Specific entropy function

$$\eta = \hat{\eta}^{te}(\boldsymbol{\varepsilon}-\boldsymbol{\varepsilon}^p, T) + \hat{\eta}^{tp}(\vartheta^p, \boldsymbol{\kappa}^p, \zeta^p, T) + \hat{\eta}^{pc}(\boldsymbol{\varepsilon}-\boldsymbol{\varepsilon}^p, T)$$

with

$$\eta^{te} = -\frac{\partial \psi^{te}}{\partial T} = -\frac{1}{2\rho_0}(\boldsymbol{\varepsilon}-\boldsymbol{\varepsilon}^p):\frac{\partial \mathbb{C}^s}{\partial T}:(\boldsymbol{\varepsilon}-\boldsymbol{\varepsilon}^p) + \frac{1}{\rho_0}(\boldsymbol{\varepsilon}-\boldsymbol{\varepsilon}^p):\mathbb{C}^s:\mathbf{1}\alpha_{th}$$
$$+\frac{1}{\rho_0}(\boldsymbol{\varepsilon}-\boldsymbol{\varepsilon}^p):\frac{\partial \mathbb{C}^s}{\partial T}:\boldsymbol{\varepsilon}^{th} + A_c + \eta_0$$

$$\eta^{tp} = -\frac{\partial \psi^{tp}}{\partial T} = \frac{1}{2\rho_0}\frac{\partial h_{\mathscr{C}^p}}{\partial T}(\vartheta^p)^2 - \frac{1}{2\rho_0}\frac{\partial h_{\mathscr{K}^p}}{\partial T}\boldsymbol{\kappa}^p:\boldsymbol{\kappa}^p + \frac{1}{\rho_0}\zeta^p$$

$$\eta^{pc} = -\frac{\partial \psi^{pc}}{\partial \mathrm{T}} = \mathrm{A}_{pc} - \frac{1}{3\rho_0}(\boldsymbol{\varepsilon}-\boldsymbol{\varepsilon}^p):\mathbb{C}^s:\mathbf{1}\delta_{pc}\frac{\partial f_{pc}}{\partial T} + \frac{1}{\rho_0}(\boldsymbol{\varepsilon}-\boldsymbol{\varepsilon}^p):\frac{\partial \mathbb{C}^s}{\partial T}:\boldsymbol{\varepsilon}^{pc}$$

Specific internal energy

$$\omega = \hat{\omega}^{te}(\boldsymbol{\varepsilon}-\boldsymbol{\varepsilon}^p, T) + \hat{\omega}^{tp}(\vartheta^p, \boldsymbol{\kappa}^p, \zeta^p, T) + \hat{\omega}^{pc}(\boldsymbol{\varepsilon}-\boldsymbol{\varepsilon}^p, T)$$

with

$$\omega^{te} = \psi^{te} - \frac{\partial \psi^{te}}{\partial T}T = \frac{1}{2\rho_0}(\boldsymbol{\varepsilon}-\boldsymbol{\varepsilon}^p):\mathbb{c}^s:(\boldsymbol{\varepsilon}-\boldsymbol{\varepsilon}^p) - \frac{1}{\rho_0}(\boldsymbol{\varepsilon}-\boldsymbol{\varepsilon}^p):\mathbb{C}^s:\boldsymbol{\varepsilon}^{th}$$
$$+\psi_c + \frac{1}{\rho_0}(\boldsymbol{\varepsilon}-\boldsymbol{\varepsilon}^p):\boldsymbol{\sigma}_0 - \eta_0(T-T_0) + \psi_0 - \frac{T}{2\rho_0}(\boldsymbol{\varepsilon}-\boldsymbol{\varepsilon}^p):\frac{\partial \mathbb{C}^s}{\partial T}:(\boldsymbol{\varepsilon}-\boldsymbol{\varepsilon}^p)$$
$$+\frac{T}{\rho_0}(\boldsymbol{\varepsilon}-\boldsymbol{\varepsilon}^p):\mathbb{C}^s:\mathbf{1}\alpha_{th} + \frac{T}{\rho_0}(\boldsymbol{\varepsilon}-\boldsymbol{\varepsilon}^p):\frac{\partial \mathbb{C}^s}{\partial T}:\boldsymbol{\varepsilon}^{th} + A_c + T\eta_0$$

$$\omega^{tp} = \psi^{tp} - \frac{\partial \psi^{tp}}{\partial T}T = -\frac{1}{2\rho_0}h_{\mathscr{C}^p}(\vartheta^p) + \frac{1}{2\rho_0}h_{\mathscr{K}^p}\boldsymbol{\kappa}^p:\boldsymbol{\kappa}^p - \frac{1}{\rho_0}T\zeta^p + \frac{T}{2\rho_0}\frac{\partial h_{\mathscr{C}^p}}{\partial T}(\vartheta^p)^2$$
$$-\frac{T}{2\rho_0}\frac{\partial h_{\mathscr{K}^p}}{\partial T}\boldsymbol{\kappa}^p:\boldsymbol{\kappa}^p + \frac{T}{\rho_0}\zeta^p$$

$$\omega^{pc} = \psi^{pc} - \frac{\partial \psi^{pc}}{\partial T}T = \psi_L - \frac{1}{\rho_0}(\boldsymbol{\varepsilon}-\boldsymbol{\varepsilon}^p):\mathbb{C}^s:\boldsymbol{\varepsilon}^{pc} + TA_{pc}$$
$$-\frac{T}{3\rho_0}(\boldsymbol{\varepsilon}-\boldsymbol{\varepsilon}^p):\mathbb{C}^s:\mathbf{1}\delta_{pc}\frac{\partial f_{pc}}{\partial T} + \frac{T}{\rho_0}(\boldsymbol{\varepsilon}-\boldsymbol{\varepsilon}^p):\frac{\partial \mathbb{C}^s}{\partial T}:\boldsymbol{\varepsilon}^{pc}$$

Box 1.—*Continued*

Tangent specific heat capacity

$$c = \hat{c}^{te}(\boldsymbol{\varepsilon}-\boldsymbol{\varepsilon}^p, T) + \hat{c}^{tp}(\vartheta^p, \boldsymbol{\kappa}^p, T) + \hat{c}^{pc}(\boldsymbol{\varepsilon}-\boldsymbol{\varepsilon}^p, T)$$

with

$$c^{te} = -T^2\frac{\partial^2\psi^{te}}{\partial T^2} = -\frac{T}{2\rho_0}(\boldsymbol{\varepsilon}-\boldsymbol{\varepsilon}^p):\frac{\partial^2\mathbb{C}^s}{\partial T^2}:(\boldsymbol{\varepsilon}-\boldsymbol{\varepsilon}^p) + \frac{2T}{\rho_0}(\boldsymbol{\varepsilon}-\boldsymbol{\varepsilon}^p):\frac{\partial\mathbb{C}^s}{\partial T}:\mathbf{1}\alpha_{th}$$

$$+\frac{T}{\rho_0}(\boldsymbol{\varepsilon}-\boldsymbol{\varepsilon}^p):\mathbb{C}^s:\mathbf{1}\frac{\partial\alpha_{th}}{\partial T} + \frac{T}{\rho_0}\frac{\partial^2\mathbb{C}^s}{\partial T^2}:\boldsymbol{\varepsilon}^{th} + c^s + \frac{\partial c^s}{\partial T}(T-T_{\mathrm{ref}})$$

$$c^{tp} = -T^2\frac{\partial^2\psi^{tp}}{\partial T^2} = \frac{T}{2\rho_0}\left[\frac{\partial^2 h_{\mathscr{C}^p}}{\partial T^2}(\vartheta^p)^2 - \frac{\partial^2 h_{\mathscr{K}^p}}{\partial T^2}\boldsymbol{\kappa}^p:\boldsymbol{\kappa}^p\right]$$

$$c^{pc} = -T^2\frac{\partial^2\psi^{pc}}{\partial T^2} - L\frac{\partial f_{pc}}{\partial T}$$

$$= -\frac{2T}{3\rho_0}(\boldsymbol{\varepsilon}-\boldsymbol{\varepsilon}^p):\frac{\partial\mathbb{C}^s}{\partial T}:\mathbf{1}\delta_{pc}\frac{\partial f_{pc}}{\partial T} - \frac{2T}{3\rho_0}(\boldsymbol{\varepsilon}-\boldsymbol{\varepsilon}^p):\mathbb{C}^s:\mathbf{1}\frac{\partial\delta_{pc}}{\partial T}\frac{\partial f_{pc}}{\partial T}$$

$$-\frac{2T}{3\rho_0}(\boldsymbol{\varepsilon}-\boldsymbol{\varepsilon}^p):\mathbb{C}^s:\mathbf{1}\delta_{pc}\frac{\partial^2 f_{pc}}{\partial T^2} + \frac{T}{\rho_0}(\boldsymbol{\varepsilon}-\boldsymbol{\varepsilon}^p):\frac{\partial^2\mathbb{C}^s}{\partial T^2}:\boldsymbol{\varepsilon}^{pc}$$

Specific internal plastic heat source

$$r^p_{\mathrm{int}} = \mathbf{r}^p_e:\dot{\boldsymbol{\varepsilon}} + r^p_T\dot{T}$$

with

$$\mathbf{r}^p_e = H(\dot{\lambda})\frac{A_r}{\rho_0}\boldsymbol{\Phi}$$

$$r^p_T = H(\dot{\lambda})\frac{A_r}{\rho_0}\chi$$

and

$$A_r = (T\boldsymbol{\beta}+\boldsymbol{\sigma}):\boldsymbol{R} + B_r$$

$$B_r = (1-f_{pc})\left[H_\vartheta\left(T\frac{\partial h_{\mathscr{C}^p}}{\partial T}\vartheta^p - \mathscr{C}^p\right) - H_\kappa\left(T\frac{\partial h_{\mathscr{K}^p}}{\partial T}\boldsymbol{\kappa}^p + \mathscr{K}^p\right):\boldsymbol{R}\right]$$

in terms of D^p_{int}

$$r^p_{\mathrm{int}} = \frac{T}{\rho_0}(\boldsymbol{\beta}:\boldsymbol{R} + A_\chi)\dot{\lambda} + \frac{1}{\rho_0}D^p_{\mathrm{int}}$$

Box 2
Tangent stress–strain relation for an isentropic process

$$\dot{\boldsymbol{\sigma}} = \mathbb{C}_{\eta}^{ep} : \dot{\boldsymbol{\varepsilon}}$$

Isentropic elasto-plastic constitutive tensor

$$\mathbb{C}_{\eta}^{ep} = \mathbb{C}_{\eta} - H(\dot{\lambda}_{\eta})(\mathbb{C}_{\eta} : \boldsymbol{R} + B_{\eta} A_{\chi} \boldsymbol{\beta}) \otimes \boldsymbol{\Phi}_{\eta}$$

Isentropic tangent elastic constitutive tensor

$$\mathbb{C}_{\eta} = \mathbb{C}^{s} + B_{\eta} \boldsymbol{\beta} \otimes \boldsymbol{\beta}$$

Isentropic plastic consistency parameter

$$\dot{\lambda}_{\eta} = \langle \boldsymbol{\Phi}_{\eta} : \dot{\boldsymbol{\varepsilon}} \rangle$$

with

$$\boldsymbol{\Phi}_{\eta} = \frac{1}{A_{\eta}} (\boldsymbol{\Phi} - \chi B_{\eta} \boldsymbol{\beta})$$

$$A_{\eta} = 1 - \chi B_{\eta} (\boldsymbol{\beta} : \boldsymbol{R} + A_{\chi})$$

$$B_{\eta} = \frac{T}{\rho_0 \left(c + L \dfrac{\partial f_{pc}}{\partial T} \right)}$$

Tangent stress–strain constitutive laws can also be obtained for different particular thermodynamical situations. For an isentropic process ($\eta = \eta_0 \Rightarrow \dot{\eta} = 0$), for instance, such constitutive law is shown in Box 2 where, if the condition $\dot{\eta}^{tp} = 0$ is additionally assumed, $A_{\chi} = 0$ should be considered in it. As it will be shown in Section 5, these isentropic constitutive tensors will play a relevant role in a specific numerical strategy usually used to solve the finite element equations of this coupled problem. Finally, note that the condition $\eta^{tp} = 1/\rho_0 \zeta^{p}$, initially proposed and extensively exploited by Armero and Simo (1992b) in thermomechanical problems without phase-change effects, is only satisfied for constant hardening properties.

3.4. Internal plastic dissipation

For the constitutive model already described, the internal plastic dissipation becomes:

$$\begin{aligned} D_{\text{int}}^{p} &= \boldsymbol{\sigma} : \dot{\boldsymbol{\varepsilon}}^{p} + \mathscr{C}^{p} \dot{\vartheta}^{p} + \mathscr{K}^{p} : \dot{\boldsymbol{\kappa}}^{p} + T \dot{\zeta}^{p} \\ &= \left\{ [\boldsymbol{\sigma} - (1 - f_{pc}) H_{\kappa} \mathscr{K}^{p}] : \boldsymbol{R} - (1 - f_{pc}) H_{\vartheta} \mathscr{C}^{p} - T \left(\frac{\partial \mathscr{C}^{th}}{\partial T} - \frac{\partial f_{pc}}{\partial T} \mathscr{C}^{p} \right) \right\} \dot{\lambda} \geqslant 0. \end{aligned} \tag{3.32}$$

This condition is automatically satisfied if there is not evolution of the internal plastic variables ($\dot{\lambda} = 0$). If this is not the case, taking into account the definitions of H_{ϑ} and H_{κ} given above, it can

be proved that $[\boldsymbol{\sigma}-(1-f_{pc})H_{\kappa}\mathscr{K}^{p}]:\boldsymbol{R}\geqslant 0$ (note, however, that the plastic work rate $\boldsymbol{\sigma}:\dot{\boldsymbol{\varepsilon}}^{p}$ proportional to $\boldsymbol{\sigma}:\boldsymbol{R}$ could be less than zero in this case) and, in order to guarantee the fulfilment of such equation, the following three sufficient conditions have to be assumed: (i) $h_{\mathscr{C}^{p}}\geqslant 0$, (ii) $\partial\mathscr{C}^{th}/\partial T\leqslant 0$ and (iii) $\partial f_{pc}/\partial T\geqslant 0$. The first condition is related to the isotropic (strain or work) hardening behaviour of the material and guarantees that $\mathscr{C}^{p}\geqslant 0$, while the second one refers to the thermal softening effect. Finally, the third condition is a constraint to be considered in the definition of f_{pc} given by eqn (3.6).

4. Finite element formulation

In the context of the finite element technique (see e.g. Hughes, 1987; Zienkiewicz and Taylor, 1989), the discrete problem can be obtained via a spatial Galerkin projection of the semidiscrete problem into a finite dimensional subspace ${}_{h}\mathscr{V}_{u}$ and ${}_{h}\mathscr{V}_{T}$ of admissible C^{0} continuous shape functions $\boldsymbol{N}_{u}\subset{}_{h}\mathscr{V}_{u}$ and $N_{T}\subset{}_{h}\mathscr{V}_{T}$, respectively. Consequently, the admissible 'algorithmic' solutions spaces ${}^{t}_{h}\mathscr{L}_{u}$ and ${}^{t}_{h}\mathscr{L}_{T}$ (for fixed time $t\in\Upsilon$), also consisting of typical C^{0} functions, are defined such that ${}^{t}_{h}\boldsymbol{u}(\boldsymbol{X})\subset{}^{t}_{h}\mathscr{L}_{u}$ and ${}^{t}_{h}T(\boldsymbol{X})\subset{}^{t}_{h}\mathscr{L}_{T}$, respectively. Making use of the standard spatial interpolation for the displacement and temperature fields, it leads to:

$$ {}^{t}_{h}\boldsymbol{u}(\boldsymbol{X})=\boldsymbol{N}_{u}(\boldsymbol{X})\,{}^{t}\boldsymbol{U}^{(e)} \tag{4.1a}$$

$$ {}^{t}_{h}T(\boldsymbol{X})=\boldsymbol{N}_{T}(\boldsymbol{X})\,{}^{t}\boldsymbol{T}^{(e)} \tag{4.1b}$$

where $\boldsymbol{N}_{u}=[\boldsymbol{N}_{u_1},\ldots,\boldsymbol{N}_{u_{n_{\text{node}}}}]$ with $\boldsymbol{N}_{u_i}=N_i\boldsymbol{I}\in{}_{h}\mathscr{V}_{u}$ and $\boldsymbol{N}_{T}=[N_{T_1},\ldots,N_{Tn_{\text{node}}}]$ with $N_{T_i}=N_i\in{}_{h}\mathscr{V}_{T}$ both for $i=1,\ldots,n_{\text{node}}$ and $e=1,\ldots,n_{\text{elem}}$.

In the above, $\boldsymbol{N}_{u}$ and $\boldsymbol{N}_{T}$ are the element shape function matrices for the displacement and temperature interpolation, respectively. Further, ${}^{t}\boldsymbol{U}^{(e)}$ is the nodal displacement vector, ${}^{t}\boldsymbol{T}^{(e)}$ is the nodal temperature vector (the superscript e denotes element values) and $\boldsymbol{I}$ is the identity matrix. It should be noted that the same finite element interpolation is used for each component of $\boldsymbol{u}$ and T. For simplicity in the notation, the subscript h will be dropped from here onwards.

Following standard procedures, the global discretized thermomechanical equations can be written in matrix form for a certain time t as:

$$\begin{aligned}&\boldsymbol{R}_{U}=\boldsymbol{F}_{U}+\boldsymbol{F}_{f}-\boldsymbol{M}\ddot{\boldsymbol{U}}-\boldsymbol{F}_{\sigma}=\boldsymbol{0}\\&\boldsymbol{R}_{T}=\boldsymbol{F}_{T}-(\boldsymbol{C}-\boldsymbol{C}_{p})\dot{\boldsymbol{T}}-\boldsymbol{K}\boldsymbol{T}-\dot{\boldsymbol{L}}_{pc}-(\boldsymbol{G}-\boldsymbol{G}_{p})\dot{\boldsymbol{U}}=\boldsymbol{0}\end{aligned} \tag{4.2}$$

where $\boldsymbol{R}_{U}$ and $\boldsymbol{R}_{T}$ are the mechanical and thermal residual vectors, respectively. The external force vector is $\boldsymbol{F}_{U}$, $\boldsymbol{F}_{f}$ is the mechanical contact vector, $\boldsymbol{M}$ is the mass matrix and $\boldsymbol{F}_{\sigma}$ denotes the internal force vector. Moreover, $\boldsymbol{F}_{T}$ is the external heat flux vector, $\boldsymbol{C}$ is the capacity matrix, $\boldsymbol{K}$ is the conductivity matrix and $\dot{\boldsymbol{L}}_{pc}$ is the phase-change vector rate. Furthermore, $\boldsymbol{G}$ is the thermoelastic coupling matrix, while $\boldsymbol{C}_{p}$ and $\boldsymbol{G}_{p}$ are coupling matrices due to plastic effects.

The time integration of the terms containing derivatives of $\boldsymbol{U}$ and $\boldsymbol{T}$ in system (4.2) is performed via the Newmark method and the generalized mid-point rule algorithm, respectively (see e.g. Hughes, 1987; Zienkiewicz and Taylor, 1989). The latter has been also used to integrate all the rate equations involved in the constitutive model presented in Section 3.

As usual, all vectors and matrices are assembled from the element contributions in the standard

Box 3
Element matrices and vectors in the discretized thermomechanical equations

$$\boldsymbol{F}_U^{(e)} = \int_{\Omega^{(e)}} \boldsymbol{N}_u^{\mathscr{T}} \boldsymbol{b}_F \, \mathrm{d}\Omega + \int_{\Gamma_\sigma^{(e)}} \boldsymbol{N}_u^{\mathscr{T}} \bar{t} \, \mathrm{d}\Gamma_\sigma + \sum_{j=1}^{n_{c_U}} \boldsymbol{F}_{c_{U_j}}^{(e)}$$

$$\boldsymbol{F}_\sigma^{(e)} = \int_{\Omega^{(e)}} \boldsymbol{B}^{\mathscr{T}} \boldsymbol{\sigma} \, \mathrm{d}\Omega$$

$$\boldsymbol{F}_f^{(e)} = \int_{\Gamma_f^{(e)}} \boldsymbol{N}_u^{\mathscr{T}} \mathbf{t}_f \, \mathrm{d}\Gamma_f$$

$$\boldsymbol{M}^{(e)} = \int_{\Omega^{(e)}} \boldsymbol{N}_u^{\mathscr{T}} \rho_0 \boldsymbol{N}_u \, \mathrm{d}\Omega$$

$$\boldsymbol{F}^{(e)} = \int_{\Omega^{(e)}} \boldsymbol{N}_T^{\mathscr{T}} \rho_0 r \, \mathrm{d}\Omega + \int_{\Gamma_q^{(e)}} \boldsymbol{N}_T^{\mathscr{T}} \bar{q} \, \mathrm{d}\Gamma_q + \int_{\Gamma_c^{(e)}} \boldsymbol{N}_T^{\mathscr{T}} h T_{\mathrm{env}} \, \mathrm{d}\Gamma_c + \sum_{j=1}^{n_{c_T}} \boldsymbol{F}_{c_{T_j}}^{(e)}$$

$$\boldsymbol{C}^{(e)} = \int_{\Omega^{(e)}} \boldsymbol{N}_T^{\mathscr{T}} \rho_0 c \boldsymbol{N}_T \, \mathrm{d}\Omega$$

$$\boldsymbol{K}^{(e)} = \int_{\Omega^{(e)}} (\nabla \boldsymbol{N}_T)^{\mathscr{T}} \boldsymbol{k} \nabla \boldsymbol{N}_T \, \mathrm{d}\Omega + \int_{\Gamma_c^{(e)}} \boldsymbol{N}_T^{\mathscr{T}} h \boldsymbol{N}_T \, \mathrm{d}\Gamma_c + \int_{\Gamma_{f_{(1)}}^{(e)}} \boldsymbol{N}_{g_T}^{\mathscr{T}} h_g \boldsymbol{N}_{g_T} \, \mathrm{d}\Gamma_f$$

$$\dot{\boldsymbol{L}}_{pc}^{(e)} = \int_{\Omega^{(e)}} \boldsymbol{N}_T^{\mathscr{T}} \rho_0 L \dot{f}_{pc} \, \mathrm{d}\Omega$$

$$\boldsymbol{C}_p^{(e)} = \int_{\Omega^{(e)}} \boldsymbol{N}_T^{\mathscr{T}} r_T^p \boldsymbol{N}_T \, \mathrm{d}\Omega$$

$$\boldsymbol{G}^{(e)} = \int_{\Omega^{(e)}} \boldsymbol{N}_T^{\mathscr{T}} T \boldsymbol{\beta}^{\mathscr{T}} \boldsymbol{B} \, \mathrm{d}\Omega$$

$$\boldsymbol{G}_p^{(e)} = \int_{\Omega^{(e)}} \boldsymbol{N}_T^{\mathscr{T}} \boldsymbol{r}_{\varepsilon}^{p\mathscr{T}} \boldsymbol{B} \, \mathrm{d}\Omega$$

with

$$\boldsymbol{N}_{g_T} = [\boldsymbol{N}_T, -\boldsymbol{N}_T]$$

$$\boldsymbol{L}_{pc}^{(e)} = \int_{\Omega^{(e)}} \boldsymbol{N}_T^{\mathscr{T}} \rho_0 L^s (f_{pc} - f_{pc_{\mathrm{ref}}}) \, \mathrm{d}\Omega$$

manner. The form of the different elemental expressions appearing in system (4.2) can be seen in Box 3, where the superscript $\mathscr{T}$ denotes the transpose symbol and $\boldsymbol{B}$ is the classical strain–displacement matrix. Besides, $\boldsymbol{F}_{c_U}$ and $\boldsymbol{F}_{c_T}$ represent the point force vector and the temperature-

dependent concentrated heat flux vector, respectively, with n_{c_U} and n_{c_T} being the corresponding number of loaded element nodes.

The mechanical boundary conditions are given by the prescribed traction vector $\boldsymbol{t}$ acting on Γ_σ and the contact traction vector $\boldsymbol{t}_f$ due to the fact that two or more bodies can interact between themselves through Γ_f such that $\Gamma_f \subset \Gamma_\sigma$. Note that $\boldsymbol{F}_f$ is zero in absence of contact effects (see e.g. Celentano et al., 1996; Wriggers and Miehe, 1992). Further, frictionless contact conditions are assumed for $\boldsymbol{t}_f$. Moreover, the thermal boundary conditions are expressed by the prescribed normal heat flux $\bar{q}$ on Γ_q and the heat transfer coefficients $h = \hat{h}(T)$ and $h_g = \hat{h}_g(T_{(i)}, g_n, p_n)$ accounting for conduction–convection–radiation phenomena (note that a unique heat transfer coefficient is assumed to include these three phenomena); the first between a body and its surrounding environment at Γ_c and the second between two bodies through $\Gamma_f(\Gamma_c \subset \Gamma_q$ and $\Gamma_f \subset \Gamma_q)$, where g_n is the so-called normal gap and p_n is the normal contact pressure. As it will be shown in Section 6, an extremely important fact in many casting simulations is that h_g may depend on g_n and p_n in order to represent the strong variations of the heat transfer rates across Γ_f for different contact conditions. Also note that the third integral of $\boldsymbol{K}$ is only evaluated in $\Gamma_{f_{(1)}}$ due to the consideration of matrix $\boldsymbol{N}_{g_T}$ in its expression. Further details about the thermomechanical contact models used in the present work can be found in Celentano et al. (1996).

It should be noted that the vector $\dot{\boldsymbol{L}}_{pc}$ contains the latent heat effect when $\dot{f}_{pc} \neq 0$ where, in this case, a non-standard spatial integration has been adopted to compute $\boldsymbol{L}_{pc}$ accurately (see Celentano et al., 1994 for more details). Finally, as expected, the plastic coupling matrices ($\boldsymbol{C}_p$ and $\boldsymbol{G}_p$) are zero if no plastic evolutions take place.

5. Solution strategy

One possible way to solve the coupled system of eqns (4.2) is via a staggered scheme (see e.g. Armero and Simo, 1992a, b; Celentano et al., 1996; Kleiber, 1991). Within this framework, different implementations are available. In particular, the so-called 'Iterative–Converged–Consecutive' strategy, widely exploited by Celentano (1994), is presented in Box 4. The objective is to find the numerical solution of the thermomechanical problem at time $t+\Delta t$ assuming a known response for time t. To this end, the coupled thermomechanical solution is obtained by solving the thermal and mechanical problems separately and checking, additionally, the global convergence criterion. Such problems are expressed by the energy and momentum equations together with the corresponding boundary constraints, initial conditions and constitutive laws. It should be noted that the strategy name given above is due to the fact that the thermomechanical solution is iteratively achieved by means of locally converged thermal and mechanical solutions obtained in a consecutive form.

In Box 4, $\Delta \boldsymbol{T}$ is the nodal temperature vector increment, j_U is the local iteration index associated to the thermal problem, $\boldsymbol{J}_{TT} = -\partial \boldsymbol{R}_T / \partial \boldsymbol{T}$ is the thermal Jacobian matrix and $\boldsymbol{I}_{TU}$ is the 'thermal interchange array' to be transferred to the mechanical problem. Similarly, $\Delta \boldsymbol{U}$ is the nodal displacement vector increment, j_U is the local iteration index associated to the mechanical problem, $\boldsymbol{J}_{UU} = -\partial \boldsymbol{R}_U / \partial \boldsymbol{U}$ is the mechanical Jacobian matrix and $\boldsymbol{I}_{UT}$ is the 'mechanical interchange array' to be transferred to the thermal problem. Moreover, j_G is the global iteration index related to the thermomechanical problem. As mentioned above, $\Delta \boldsymbol{U}$ and $\Delta \boldsymbol{T}$ are computed separately.

Box 4
Staggered scheme for coupled thermomechanical problems: 'Iterative–Converged–Consecutive' strategy

Thermomechanical problem at time $t+\Delta t$:

Initial conditions:

$${}^{t+\Delta t}\boldsymbol{T}^{0,0} = {}^{t}\boldsymbol{T}$$

$${}^{t+\Delta t}\boldsymbol{U}^{0,0} = {}^{t}\boldsymbol{U}$$

Global iterative solution:

- thermal problem (heat balance equation)
- mechanical problem (momentum equation)
- global convergence

$\Big\}\ j_G = 0, \ldots, n_{\mathrm{iter}_G}$

- thermal problem (heat balance equation)

input:

$${}^{t+\Delta t}\boldsymbol{I}_{UT}^{j_U,j_G} = [{}^{t+\Delta t}\boldsymbol{\varepsilon}^{j_U,j_G}, {}^{t+\Delta t}\dot{\boldsymbol{\varepsilon}}^{j_U,j_G}, {}^{t+\Delta t}\boldsymbol{\varepsilon}^{pj_U,j_G}, {}^{t+\Delta t}\vartheta^{pj_U,j_G},$$

$${}^{t+\Delta t}\boldsymbol{\kappa}^{pj_U,j_G}, {}^{t+\Delta t}g_n^{j_U,j_G}, {}^{t+\Delta t}p_n^{j_U,j_G}]$$

local iterative solution:

$$\left.\begin{aligned} &{}^{t+\Delta t}\boldsymbol{J}_{TT}^{j_U-1,j_G}\boldsymbol{\Delta T}^{j_U,j_G} = {}^{t+\Delta t}\boldsymbol{R}_T^{j_U-1,j_G} \\ &{}^{t+\Delta t}\boldsymbol{T}^{j_U,j_G} = {}^{t+\Delta t}\boldsymbol{T}^{j_U-1,j_G} + \boldsymbol{\Delta T}^{j_U,j_G} \\ &\frac{\|{}^{t+\Delta t}\boldsymbol{R}_T^{j_U,j_G}\|_2}{\|{}^{t+\Delta t}\boldsymbol{F}_T\|_2} < \varepsilon_{R_T} \end{aligned}\right\} j_U = 1, \ldots, n_{\mathrm{iter}_T}$$

output:

$${}^{t+\Delta t}\boldsymbol{I}_{TU}^{j_U,j_G} = [{}^{t+\Delta t}\boldsymbol{T}^{j_U,j_G}, {}^{t+\Delta t}\dot{\boldsymbol{T}}^{j_U,j_G}, {}^{t+\Delta t}f_{pc}^{j_U,j_G}]$$

$${}^{t+\Delta t}\boldsymbol{T}^{0,j_G+1} = {}^{t+\Delta t}\boldsymbol{T}^{j_U,j_G}$$

The main features of this staggered scheme are:

—a proper interchange of variables is performed between the two problems with the sake of computing all the thermomechanical coupling effects. The interchange arrays are: $\boldsymbol{I}_{TU} = [T, \dot{T}, f_{pc}]$ and $\boldsymbol{I}_{UT} = [\boldsymbol{\varepsilon}, \dot{\boldsymbol{\varepsilon}}, \boldsymbol{\varepsilon}^p, \vartheta^p, \boldsymbol{\kappa}^p, g_n, p_n]$. Note that the global iteration index j_G only increases when the two interchanges take place,

—a global convergence criteria is adopted for the coupled thermomechanical problem due to the highly non-linearities existing in it. Therefore, it is assumed that a converged thermomechanical solution is achieved when the two conditions shown in Box 4 are fulfilled for the same j_G($\|\cdot\|_2$ is the L_2 vector norm, and ε_{R_T} and ε_{R_U} are the thermal and mechanical measures of the admissible out-of-balance residuals, respectively),

Box. 4.—*Continued*

• mechanical problem (momentum equation)

input:

$$ {}^{t+\Delta t}\boldsymbol{I}_{TU}^{j_U j_G} = [{}^{t+\Delta t}\boldsymbol{T}^{j_U j_G}, {}^{t+\Delta t}\dot{\boldsymbol{T}}^{j_U j_G}, {}^{t+\Delta t}f_{pc}^{j_U j_G}] $$

local iterative solution:

$$ \left.\begin{aligned} & {}^{t+\Delta t}\boldsymbol{J}_{UU}^{j_U-1, j_G}\Delta\boldsymbol{U}^{j_U j_G} = {}^{t+\Delta t}\boldsymbol{R}_U^{j_U-1, j_G} \\ & {}^{t+\Delta t}\boldsymbol{U}^{j_U j_G} = {}^{t+\Delta t}\boldsymbol{U}^{j_U-1, j_G} + \Delta\boldsymbol{U}^{j_U j_G} \\ & \frac{\|{}^{t+\Delta t}\boldsymbol{R}_U^{j_U j_G}\|_2}{\|{}^{t+\Delta t}\boldsymbol{F}_U\|_2} < \varepsilon_{R_U} \end{aligned}\right\} j_U = 1, \ldots, n_{\text{iter}_U} $$

output:

$$ {}^{t+\Delta t}\boldsymbol{I}_{UT}^{j_U j_G} = [{}^{t+\Delta t}\boldsymbol{\varepsilon}^{j_U j_G}, {}^{t+\Delta t}\dot{\boldsymbol{\varepsilon}}^{j_U j_G}, {}^{t+\Delta t}\boldsymbol{\varepsilon}^{pj_U j_G}, {}^{t+\Delta t}\vartheta^{pj_U j_G}, $$

$$ {}^{t+\Delta t}\boldsymbol{\kappa}^{pj_U j_G}, {}^{t+\Delta t}g_n^{j_U j_G}, {}^{t+\Delta t}p_n^{j_U j_G}] $$

$$ {}^{t+\Delta t}\boldsymbol{U}^{0, j_G+1} = {}^{t+\Delta t}\boldsymbol{U}^{j_U j_G} $$

• global convergence

$$ \frac{\|{}^{t+\Delta t}\boldsymbol{R}_U^{j_U j_G}\|_2}{\|{}^{t+\Delta t}\boldsymbol{F}_U\|_2} < \varepsilon_{R_U} $$

$$ \frac{\|{}^{t+\Delta t}\boldsymbol{R}_T^{j_U j_G}\|_2}{\|{}^{t+\Delta t}\boldsymbol{F}_T\|_2} < \varepsilon_{R_T} $$

—if only $\boldsymbol{I}_{TU}$ exists, the problem is thermally unidirectional coupled. In this case, $n_{\text{iter}_G} = 1$ where $\boldsymbol{I}_{TU}$ contains converged values,
—the problem is bidirectional coupled when $\boldsymbol{I}_{TU}$ and $\boldsymbol{I}_{UT}$ are performed.

The Jacobian matrices used in this staggered scheme for the isothermal, adiabatic and improved isothermal partitions can be found in Box 5. These partitions are fractional step methods associated with a two phase operator split of the full non-linear thermomechanical system (4.2) into a thermal phase at fixed configuration followed by an isothermal or adiabatic mechanical phase. The isothermal partition is only conditionally stable while the adiabatic split preserves the unconditional stability property characteristic of fully implicit (monolithic) schemes (see e.g. Armero and Simo, 1992a, b). However, as reported by Celentano (1994) for a simpler model than the one proposed here, the improved isothermal split is stable even when the coupling stability conditions of the numerical solution when using the isothermal partition for quasi-static and dynamic problems are violated.

Some simplificative assumptions have been considered in the derivation of $\boldsymbol{J}_{TT}$ by neglecting the

Box 5
Jacobian matrices for different partitions

• isothermal split:

$$\boldsymbol{J}_{TT} = \boldsymbol{K} + \frac{1}{\Delta t}(\boldsymbol{C} + \boldsymbol{C}_{pc} - \boldsymbol{C}_{p})$$

$$\boldsymbol{J}_{UU} = \boldsymbol{K}_{U} + \boldsymbol{K}_{f}$$

• adiabatic split:

$$\boldsymbol{J}_{TT} = \boldsymbol{K} + \frac{1}{\Delta t}(\boldsymbol{C} + \boldsymbol{C}_{pc} - \boldsymbol{C}_{p})$$

$$\boldsymbol{J}_{UU} = \boldsymbol{K}_{U_{\eta}} + \boldsymbol{K}_{f}$$

• improved isothermal split:

$$\boldsymbol{J}_{TT} = \boldsymbol{K} + \frac{1}{\Delta t}(\boldsymbol{C} + \boldsymbol{C}_{pc} - \boldsymbol{C}_{p} + \boldsymbol{C}_{th})$$

$$\boldsymbol{J}_{UU} = \boldsymbol{K}_{U} + \boldsymbol{K}_{f}$$

temperature dependence of the thermal properties and external actions. The element contributions of the matrices involved in the Jacobian expressions are shown in Box 6, where $\boldsymbol{K}_{U}$ is the stiffness matrix, $\boldsymbol{K}_{U_{\eta}}$ is the isentropic stiffness matrix, $\boldsymbol{K}_{f}$ is the contact matrix, $\boldsymbol{C}_{pc}$ is the phase-change matrix and $\boldsymbol{C}_{th}$ is the thermal coupling matrix (tr is the trace symbol) which is obtained by performing the additive strain decomposition of the thermoelastic coupling term $\boldsymbol{G}\dot{\boldsymbol{U}}$.

Once more, the evaluation of $\boldsymbol{K}_{f}$ is only done at the boundary $\Gamma_{f_{(1)}}$ due to the consideration of matrix $\boldsymbol{N}_{g_u}$ in its expression. The normal asperity stiffness E_n guarantees the perfect impenetrability condition as $E_n \to \infty$. The derivation of the contact constitutive tensor $\mathbb{C}^{f}$ is straightforward for $g_n < 0$ and the open normal gap situation given by $g_n > 0$. It should be noted, however, that for the particular case of $g_n = 0$, a regularized tensor is used in order to avoid numerical oscillations. Moreover, an exhaustive study on the computation of $\boldsymbol{C}_{pc}$, which is crucial for the convergence and stability of the thermal numerical solution, can be found in Celentano et al. (1994).

Finally, in this context, the quadratic convergence of the Newton–Raphson's method may not be achieved. Nevertheless, the thermal and mechanical residuals are 'exactly' (within the numerical frame) evaluated leading to a conservative formulation in the weak form sense.

6. Numerical examples

6.1. A unidirectional solidification example

A unidirectional solidification problem, previously analyzed by Heinlein et al. (1986) and Zabaras et al. (1990), is here undertaken in order to show the performance of the proposed

Box 6
Element matrices appearing in the Jacobian expressions

$$\boldsymbol{K}_U^{(e)} = \int_{\Omega^{(e)}} \boldsymbol{B}^{\mathscr{T}} \mathbb{C}^{ep} \boldsymbol{B} \, \mathrm{d}\Omega$$

$$\boldsymbol{K}_{U_\eta}^{(e)} = \int_{\Omega^{(e)}} \boldsymbol{B}^{\mathscr{T}} \mathbb{C}_\eta^{ep} \boldsymbol{B} \, \mathrm{d}\Omega$$

$$\boldsymbol{K}_f^{(e)} = \int_{\Gamma_{F_{(1)}}^{(e)}} \boldsymbol{N}_{g_u}^{\mathscr{T}} \mathbb{C}^f \boldsymbol{N}_{g_u} \, \mathrm{d}\Gamma_f$$

$$\boldsymbol{C}_{pc}^{(e)} = \int_{\Omega^{(e)}} \boldsymbol{N}_T^{\mathscr{T}} \rho_0 L \frac{\partial f_{pc}}{\partial T} \boldsymbol{N}_T \, \mathrm{d}\Omega$$

$$\boldsymbol{C}_{th}^{(e)} = \int_{\Omega^{(e)}} \boldsymbol{N}_T^{\mathscr{T}} T \, \mathrm{tr}(\boldsymbol{\beta}) \alpha_{th} \boldsymbol{N}_T \, \mathrm{d}\Omega$$

with

$$\boldsymbol{N}_{g_u} = [\boldsymbol{N}_u, -\boldsymbol{N}_u]$$

$$\mathbb{C}^f = \begin{cases} \boldsymbol{n}_{(1)} \boldsymbol{E}_{nu}^{\mathscr{T}} & \text{for } g_n < 0 \\ \mathbb{C}_r^f & \text{for } g_n = 0 \\ \boldsymbol{0} & \text{for } g_n > 0 \end{cases}$$

$$\boldsymbol{E}_{nu} = E_n \mathbf{n}_{(1)}$$

Table 1
Thermal properties of the aluminium

- Density: $\rho_0 = 2650.0$ [kg/m^3]
- Specific heat: $c = 0.2526$ [kcal/kg°C]
- Heat conductivity: $k = 0.0548$ [kcal/ms°C]
- Latent heat: $L = 94.44$ [kcal/kg]
- Melting temperature: $T_m = 660$ [°C]

model. The geometry of the problem is a rectangular region (width = 0.01 m in the x direction, height = 0.25 m in the y direction and unit thickness) initially occupied with high purity liquid aluminium at the melting temperature T_m. The thermal and mechanical properties of the aluminium are listed in Tables 1 and 2, respectively. For this material, $f_{pc} = H(T - T_m)$ (H being the Heaviside function). Plane strain conditions have been assumed and a particular definition of the inelastic deformation rate is used (see Zabaras et al., 1990):

Table 2
Mechanical properties of the aluminium

- Poisson ratio: $v = 0.37$

- Young modulus:

E [Mpa]	T [°C]
6.93×10^4	0.0
4.0458×10^4	660.0

- Tangent thermal dilatation coefficient:

α_{th} [1/°C]	T [°C]
23.19×10^{-6}	25.0
27.86×10^{-6}	300.0
30.23×10^{-6}	400.0
38.355×10^{-6}	660.0

- Coefficients of constitutive law:

Coefficient	Value
A_z	0.382×10^{12} [s^{-1}]
B_z	0.037 [MPa^{-1}]
C_z	18849 [°K]
n_z	3.84

The variations of E and α_{th} have been assumed to be piecewise linear within the mentioned temperatures. Below the lowest and above the highest temperatures, the properties are assumed to remain constant at the same value defined for the extreme temperature.

$$\dot{\boldsymbol{\varepsilon}}^p = \frac{3}{2} A_z \, \mathrm{e}^{-\frac{C_z}{T+273}} \frac{[\sinh(B_z \bar{\sigma})]^{n_z}}{\bar{\sigma}} \boldsymbol{\sigma}', \tag{6.1}$$

where A_z, B_z, C_z and n_z are material constants, $\bar{\sigma} = \sqrt{3J_2}$ ($J_2 = 1/2\boldsymbol{\sigma}' : \boldsymbol{\sigma}'$) is the effective stress, the temperature T must be in degrees Celsius, no hardening effects are considered and, moreover, $\delta^s_{pc} = 0$ is adopted. Note that this evolution equation is similar to (3.1) with $\dot{\lambda} = A_z \, \mathrm{e}^{-[C_z/(T+273)]} [\sinh(B_z \bar{\sigma})]^{n_z}$. The boundaries at $x = 0$ and $x = 0.01$ m are insulated and restrained from motion in the x-direction while the side $y = 0$ is fixed. A temperature cooling boundary condition of the following form is applied at $y = 0$:

$$\bar{T} = T_a + (T_m - T_a) \, \mathrm{e}^{-Rt}, \tag{6.2}$$

where $T_a = 300$°C is the final steady-state temperature and $R = 0.023$ s^{-1} is a cooling parameter. Twenty-five four-noded isoparametric elements have been used in this example with a time step of 20 s.

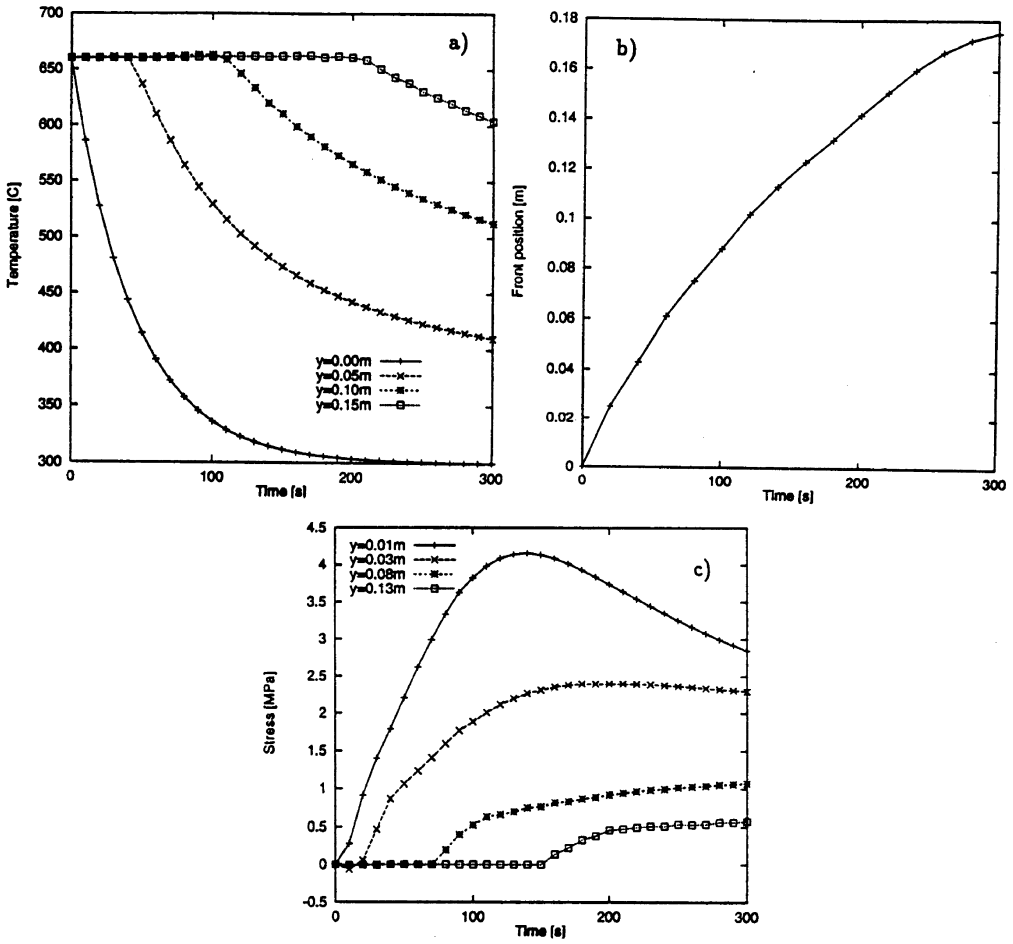

Fig. 1. A unidirectional solidification example: (a) temperature evolutions at different locations, (b) phase-change front position evolution and (c) lateral stress evolution at different locations.

The temperature evolution at different locations is shown in Fig. 1(a). The phase-change front position history is plotted in Fig. 1(b). All these results are in perfect agreement with those reported by Heinlein et al. (1986) and Zabaras et al. (1990). The computed lateral stress histories at various points are presented in Fig. 1(c). As shown in this last figure, the lateral stress is in general tensile and builds up any location with the arrival of the front due to thermal contractions. Further, it can be seen that the stress near $y = 0$ eventually relaxes while away from this boundary the stresses are smaller due to the low temperature rate. Once more, these results are very similar to those reported by Heinlein et al. (1986) and Zabaras et al. (1990).

6.2. *Solidification of a circular cylinder*

The solidification of an axially symmetric cylinder (radius = 0.018 m and height = 0.001 m) initially filled with liquid aluminium at melting temperature is analyzed. For this problem, studied

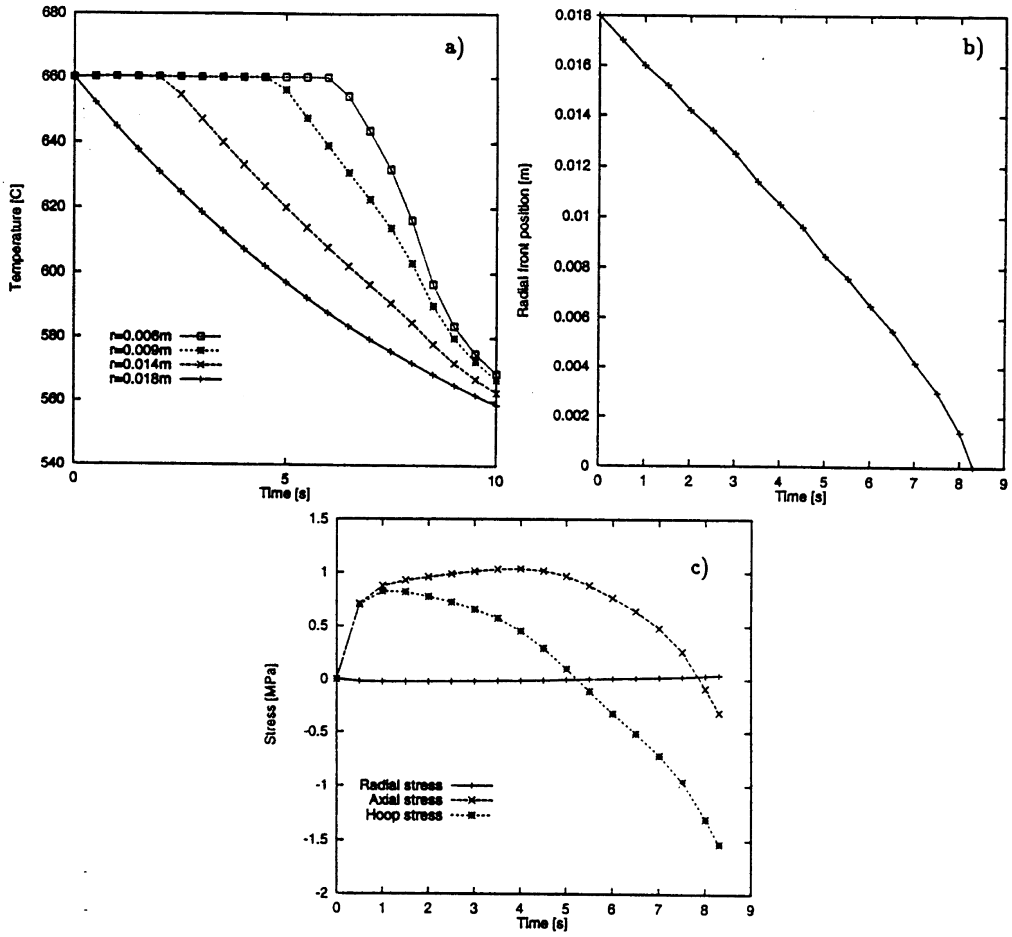

Fig. 2. Solidification of a circular cylinder: (a) temperature evolutions at different locations, (b) phase-change front position evolution and (c) stress evolution at $r = 0.018$.

by Zabaras et al. (1990, 1991), the thermomechanical material properties are the same as those employed in the first example. Plane strain conditions in the axial direction with a traction-free outer surface ($r = 0.018$ m) have been assumed and eqn (6.1) is adopted to describe the inelastic strain rate. The top and bottom are insulated while the outer surface is cooled with the temperature history depicted in eqn (6.2) with $T_a = 500°C$ and $R = 0.1\ s^{-1}$. The finite element mesh considered in the analysis consisted of eighteen four-noded isoparametric elements. The time step chosen was 0.5 s.

The temperature history at various locations and the phase-change front position are, respectively, shown in Fig. 2(a) and (b). These results are in excellent agreement to those reported by Zabaras et al. (1990). The radial, axial and hoop stress evolution up to the solidification time (approximately 8.3 s) at $r = 0.018$ m are presented in Fig. 2(c). As seen from this figure, at the end of the solidification both the hoop and axial stresses are compressive at the outer surface. The trend of the stresses found in this paper is similar to that reported by Smelser and Richmond (1998) and in a good quantitative agreement with the results obtained by Zabaras et al. (1990).

6.3. Light alloy solidification in a permanent composite mould: experimental validation

In a casting situation where an aluminium alloy solidifies in a permanent mould, a gap initiates and grows between the shrinking casting and the mould (see e.g. Gunasegaram et al., 1995; Nishida et al., 1986). It is well known that the formation of this gap results in a substantial reduction in heat transfer rates across the casting–mould interface and hence is an important factor in solidification studies. Due to the thermomechanical nature of the gap formation, it has long been recognized that a purely thermal analysis cannot properly represent this fact (see e.g. Bellet et al., 1993, 1996; Celentano, 1994; Celentano et al., 1995, 1996; Chow et al., 1995; Gunasegaram et al., 1997; Smelser and Richmond, 1988; Trovant and Argyropoulos, 1996; Vicente-Hernandez et al., 1995). Other topics of interest are the description of the thermomechanical behaviour of the alloy and the mould during the whole process with a special emphasis on the phase-change effects occurring in the alloy solidification range, and the influence of selected casting parameters (e.g., mould preheat) on the solidification pattern.

The objective of this section is the experimental validation of the present thermomechanical formulation in the analysis of the solidification process of an aluminium alloy in a permanent composite mould. In the experiments (see Gunasegaram et al., 1997), commercial aluminium alloy Al-7 Si-0.3 Mg was gravity cast in a composite permanent mould made of H13 hot work steel and beryllium copper (BeCu, ASTM: C17510) along with insulating tombo marine board. The overall experimental set up is shown in Fig. 3. The casting geometry was a stepped vertical cylindrical block. The permanent composite mould comprises materials selected on the basis of their thermal properties and assembled and operated in such a way as to promote directional solidification of the casting. The metallic components of the mould were bolted onto each other. The H13 (bottom) component was bolted down to a base via through-holes drilled in the tombo insulation. No mould coat was used, except at the casting-H13 feeder interface and mould–mould interfaces where an insulating ladle coat was applied. The temperature-dependent thermophysical and mechanical properties of all these materials can be found in Tables 3 and 4, respectively. In particular, an experimental-based solid fraction-temperature relationship with a temperature-dependent specific latent heat value has been considered in the simulations.

Several thermocouples (TC) were inserted in the casting and the mould in order to obtain temperature histories (see Fig. 3). It may be noted that those labelled 1–9 were chosen since they were the most relevant. In particular, TC 1–6 were located in the same horizontal planes (A and B) of the linear variable displacement transformer (LVDT) probes detecting casting and mould radial displacement evolutions at the interface. Further details of the data acquisition system may be found in Gunasegaram et al. (1995), 1997).

Two different experiments have been performed to evaluate the effect of low and high mould preheat cases (experiments I and II, respectively) on the initiation time and growth rate of the normal gap.

In these experiments, the correlation between the measured normal gap size (calculated as the difference between the measured displacements of the corresponding surfaces of the casting and the mould) and the casting–mould interfacial heat transfer coefficient (i.e., the $h_g = \hat{h_g}(g_n)$ relationship) was obtained in Gunasegaram et al. (1997) by solving the inverse heat conduction problem. The same methodology was used in the derivation of the mould-ambient heat transfer coefficients. The obtained heat transfer coefficients at the different interfaces are presented in Table 5. It should

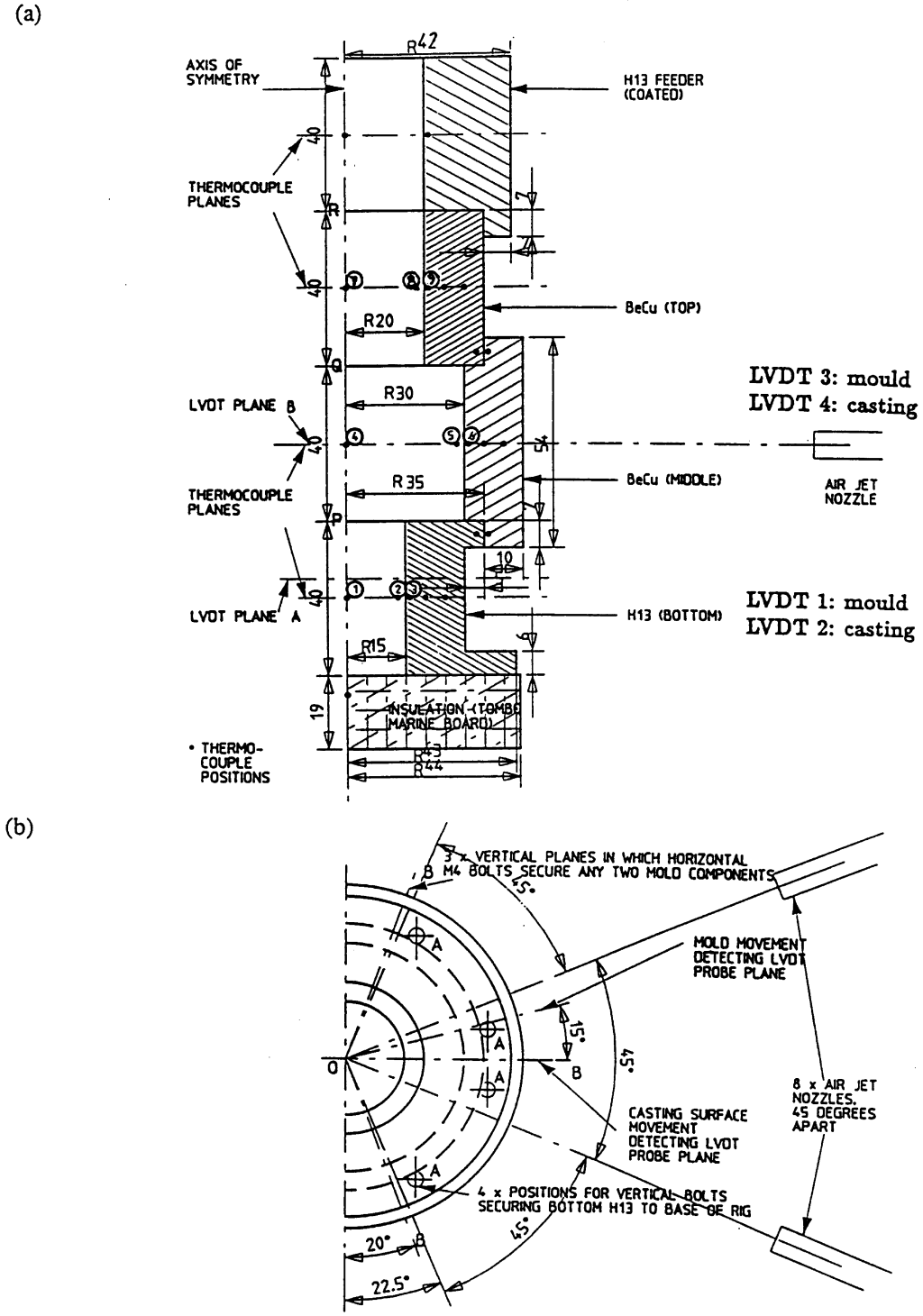

Fig. 3. Validation test: experimental set up: (a) half section elevation and (b) top view. All dimensions in mm. Thermocouple numbers are shown within circles.

Table 3
Thermal properties of the materials used in the experiments

Thermal properties of casting alloy

- Density:

$\rho \times 10^3$ [kg/m^3]	T [°C]
2.68	500
2.58	545
2.58	607.8
2.53	611

- Tangent specific heat:

c [J/kg°K]	T [°C]
876	0.0
926	100
972	200
1017	300
1061	400
1105	500
1125	545
1125	555
1085	611

- Conductivity:

k [J/ms°K]	T [°C]
160	0
150	100
140	400
150	555
134	568
116	570
98	603
95	608
100	611
200	620
300	650
500	750

- Solid fraction:

$(1-f_{pc})$	T [°C]	$L \times 10^3$ [J/kg]
1.000	545	495
0.910	555	495
0.829	563	495
0.805	564	495
0.736	565	398
0.550	566	398
0.405	589	398
0.194	611	398
0.137	614	398
0.000	615	398

The variations of ρ, c, k, $(1-f_{pc})$ and L have been assumed to be piecewise linear within the mentioned temperatures. Below the lowest and above the highest temperatures, the properties are assumed to remain constant at the same value defined for the extreme temperature.

Table 3.—*Continued*

Thermal properties of H13 steel

- Density: 7626 [kg/m^3]
- Tangent specific heat:

c [J/kg°K]	T [°C]
450	23
465	50
474	75
481	100
488	125
496	150
504	175
512	200
521	225
531	250
542	275
554	300
567	325
583	350
598	375
610	400
623	425
637	450
653	475
673	500
698	525
723	550
749	575
770	600
926	700

- Conductivity:

k [J/ms°K]	T [°C]
21.037	20
22.889	100
24.716	200
26.237	300
27.307	400
27.336	500
27.968	600

The variations of c and k have been assumed to be piecewise linear within the mentioned temperatures. Below the lowest and above the highest temperatures, the properties are assumed to remain constant at the same value defined for the extreme temperature.

Table 3.—*Continued*

Thermal properties of BeCu steel

- Density: 8750 [kg/m^3]
- Tangent specific heat:

c [J/kg°K]	T [°C]
395	23
400	50
404	75
408	100
412	125
415	150
417	175
419	200
421	225
423	250
425	275
427	300
429	325
432	350
434	375
436	400
438	425
441	450
443	475
445	500
447	525
449	550
450	575
451	600
453	625
455	650

- Conductivity:

k [J/ms°K]	T [°C]
260.246	23
277.736	100
292.556	200
301.131	300
309.385	400
307.595	500
306.218	600
308.934	650

The variations of c and k have been assumed to be piecewise linear within the mentioned temperatures. Below the lowest and above the highest temperatures, the properties are assumed to remain constant at the same value defined for the extreme temperature.

Table 3.—*Continued*

Thermal properties of Tombo

- Density: 660 [kg/m^3]
- Specific Heat: 1130 [J/kg°K]
- Conductivity:

k [J/ms°K]	T [°C]
0.080	100
0.085	200
0.095	300
0.105	400
0.120	500

The variations of k have been assumed to be piecewise linear within the mentioned temperatures. Below the lowest and above the highest temperatures, the properties are assumed to remain constant at the same value defined for the extreme temperature.

be noted that, in general, different values for these coefficients have been derived for each mould component.

A structured 2-D finite element mesh composed of about 550 axisymmetric four-noded isoparametric quadrilateral elements has been used for the numerical analysis of this problem. The simulations have been carried out with VULCAN (see Celentano, 1996), a fully coupled thermomechanical finite element code in which the constitutive models presented in this work have been implemented. The bidirectional coupling numerical strategy shown in Box 4 was employed in the analysis where, additionally, it can be demonstrated that the isothermal split is stable for this problem since its coupling stability conditions are not violated. Moreover, the current study does not include fluid flow and hence assumes instantaneous fill of the mould cavity.

The mechanical boundary conditions used in the simulations take into account the effects of the bolts joining the mould components (no relative displacement between mould materials at interfaces) and the G-clamp placed on the upper part of the H13 feeder (no displacement at external faces of the feeder in the horizontal plane corresponding to the clamp's position). Moreover, a frictionless contact model with $E_n = 10^{10}$ MPa/mm is considered at the casting–mould interfaces.

In the experiments, an air/gas mixture was used for mould preheating. The initial temperatures attained by the casting and the various components of the composite mould for the experiments I and II are given in Table 6.

Figure 4 shows the experimentally measured and computed temperature histories while the radial displacement and normal gap evolutions are presented in Fig. 5, both for experiment I. Additionally, similar results are presented in Figs 6 and 7 for experiment II.

As it can be seen in Figs 4 and 6, satisfactory agreement is obtained between experimental and simulated temperature evolutions for both cases. In particular, a reasonably good description is achieved in the phase-change region.

It is found in the experiments that the gap initiates when the alloy temperature close to the

Table 4
Mechanical properties of the materials used in the experiments

Mechanical properties of casting alloy

- Poisson ratio: $\nu = 0.33$
- Young modulus:

E [MPa]	T [°C]
72.4×10^3	25.0
1.0×10^3	545.0

- Secant thermal dilatation coefficient:

$\alpha^s_{th} \times 10^{-6}$ [1/°C]	T [°C]
21.5	100.0
22.5	200.0
23.5	300.0

- Thermal hardening function:

$\mathscr{C}_{th}$ [MPa]	T [°C]
100	25.0
0.01	545.0

- Isotropic hardening modulus: 100 [MPa]
- Kinematic hardening modulus: 100 [MPa]
- Secant phase-change volumetric deformation: 0.01

The variations of E, α^s_{th} and $\mathscr{C}_{th}$ have been assumed to be piecewise linear within the mentioned temperatures. Below the lowest and above the highest temperatures, the properties are assumed to remain constant at the same value defined for the extreme temperature.

casting surface falls to approximately 540°C, nearly independent of mould preheat, mould material, cooling rate, casting section radius and/or metallostatic head. This effect is closely related to the hardening development characteristics during the alloy solidification (see e.g. Singer and Cotrelli, 1946).

As may be seen in Figs 5 and 7, the gaps do not initiate until the casting surface follows the mould surface due to lack of strength in the solidifying casting. Although good qualitative agreement between measured and numerically predicted radial displacement and gap evolutions has been obtained, the quantitative fitting is only reasonable. Reasons for this deviation may be due to the approximate nature of the thermal hardening function-temperature relationship used for the casting alloy at high temperatures (particularly in the mushy zone), the accuracy in the heat transfer coefficients considered in the analysis, the assumption of uniform initial temperature distribution for the casting and every component of the mould and the inward flexing of the

Table 4.—*Continued*

Mechanical properties of H13 steel

- Poisson ratio: $\nu = 0.30$
- Young modulus: 216×10^3 [MPa]
- Secant thermal dilatation coefficient:

$\alpha^s_{th} \times 10^{-6}$ [1/°C]	T [°C]
11.5	100.0
12.0	200.0
12.2	300.0
12.5	400.0
12.8	500.0
13.0	600.0

- Thermal hardening function:

$\mathscr{C}_{th}$ [MPa]	T [°C]
1005	425.0
820	540.0
690	595.0
350	650.0

The variations of α^s_{th} and $\mathscr{C}_{th}$ have been assumed to be piecewise linear within the mentioned temperatures. Below the lowest and above the highest temperatures, the properties are assumed to remain constant at the same value defined for the extreme temperature.

Mechanical properties of BeCu steel

- Poisson ratio: $\nu = 0.28$
- Young modulus: 132.5×10^3 [MPa]
- Secant thermal dilatation coefficient: 17.6×10^{-6} [1/°C]
- Thermal hardening function:

$\mathscr{C}_{th}$ [MPa]	T [°C]
760	20.0
260	200.0

The variations of $\mathscr{C}_{th}$ have been assumed to be piecewise linear within the mentioned temperatures. Below the lowest and above the highest temperatures, the properties are assumed to remain constant at the same value defined for the extreme temperature.

Mechanical properties of Tombo

- Poisson ratio: $\nu = 0.30$
- Young modulus: 2.8×10^3 [MPa]
- Secant thermal dilatation coefficient: 0.0 [1/°C]
- Thermal hardening function: 0.084 [MPa]

Table 5
Heat transfer coefficients at the different interfaces

Thermal boundary conditions		
Interface	Heat transfer coefficient [W m^{-2} K^{-1}]	
H13 (bottom)—air	30	
BeCu (middle)—air	30	
BeCu (top)—air	30	
H13 (feeder)—air	30	
Tombo—air	20	
Casting—air	50	
H13 (bottom)—casting:		
		g_n [mm]
	10,000	0.000
	4500	0.005
	3000	0.010
	2000	0.015
	1500	0.030
BeCu (middle and top)—casting:		
		g_n [mm]
	8000	0.000
	2800	0.005
	1600	0.010
	1200	0.015
H13 (feeder)—casting:	700	
Casting—Tombo	400	
H13 (bottom)—Tombo	250	
H13 (bottom)—BeCu (middle)	2000	
BeCu (middle)—BeCu (top)	2000	
BeCu (top)—H13 (feeder)	2000	

The variations of h have been assumed to be piecewise linear within the mentioned gaps. Below the lowest and above the highest gaps, the values of h are assumed to remain constant at the same value defined for the extreme gap.

mould as soon as the melt is poured into the cavity. Note, however, that the numerical solutions approximately adjust the measured initiation times of the normal gap.

For these experiments, it is also observed that the rate of growth of the gap width is greater in the lower mould preheat case (Figs 5 and 7). The cause for the latter is shown to be the combined effect of a higher casting shrinkage rate and a larger mould expansion rate. It can be seen that the numerical solution approaches the experimental values. It should be also noted that below a certain mould preheat, for a given mould material, not much reduction in solidification times was obtained due to the drastic decrease of h_g once a normal gap is developed.

Table 6
Initial temperatures (°C) for the experiments I and II

Material	Experiment I	Experiment II
Casting alloy	655	685
H13 (bottom)	195	399
BeCu (middle)	236	487
BeCu (top)	245	513
H13 (feeder)	246	573
Tombo insulation	133	291

The gap initiates earlier in the BeCu (middle) part of the mould than in the H13 (bottom) part when the preheat is lower (experiment I, Fig. 5) but later when the preheat is higher (experiment II, Fig. 7). These phenomena can be, respectively, explained by the better early chilling capabilities of BeCu and the different preheats of BeCu (middle) and H13 (bottom) for experiment II (see Table 6).

7. Conclusions

A coupled thermomechanical model to simulate the light alloy solidification process in a permanent composite mould has been presented. The model is formulated within the plasticity theory framework and accounts for the different behaviours of the materials involved in the problem. To this end, a set of appropriate internal variables and a specific free energy function have been proposed in order to derive the secant and tangent expressions for all the constitutive laws. The main features of such equations are the consideration of an experimental-based phase-change function, a temperature-dependent specific latent heat value and a phase-change strain tensor.

The corresponding finite element formulation standing out the importance of the variable thermomechanical boundary conditions occurring in the problem has also been presented.

Special attention has been devoted to the numerical strategy used to solve the highly non-linear coupled system of equations. An enhanced staggered scheme allowing the consideration of different partitions has been used.

The model has been used in the simulation of two simple casting examples previously analysed by other researchers. Moreover, the model has been also validated with laboratory measurements obtained during an experimental test where satisfactory agreement between numerical and experimental results can be observed for different casting situations. However, further research in the thermomechanical material description specially at high temperatures is still necessary in order to achieve even more realistic numerical responses.

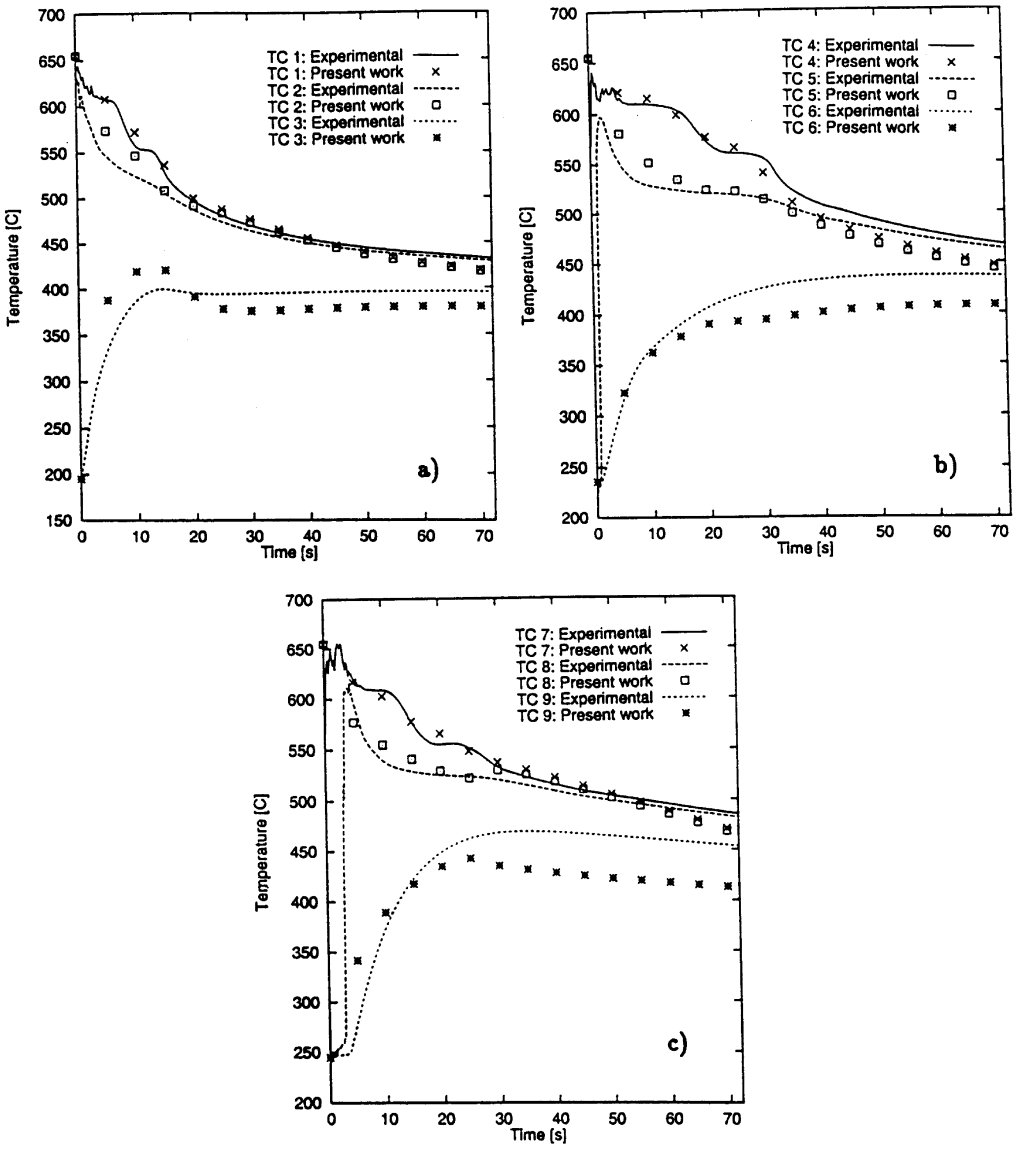

Fig. 4. Validation test: temperature evolutions for the experiment I: (a) thermocouples 1, 2 and 3, (b) thermocouples 4, 5 and 6 and (c) thermocouples 7, 8 and 9.

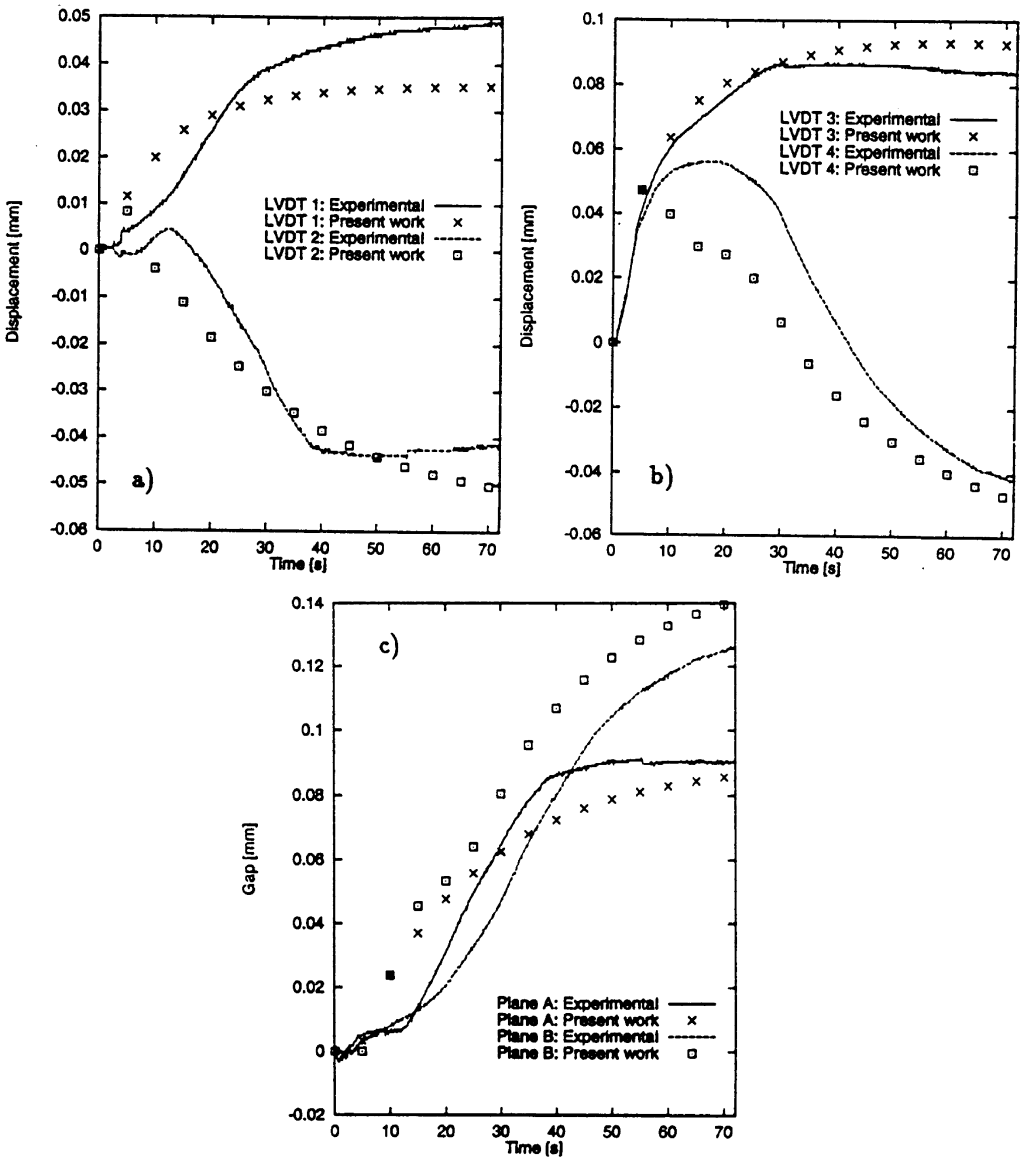

Fig. 5. Validation test: radial displacement evolutions for the experiment I: (a) LVDTs 1 and 2 and (b) LVDTs 3 and 4. Normal gap evolutions for the experiment I: (c) LVDT planes A and B.

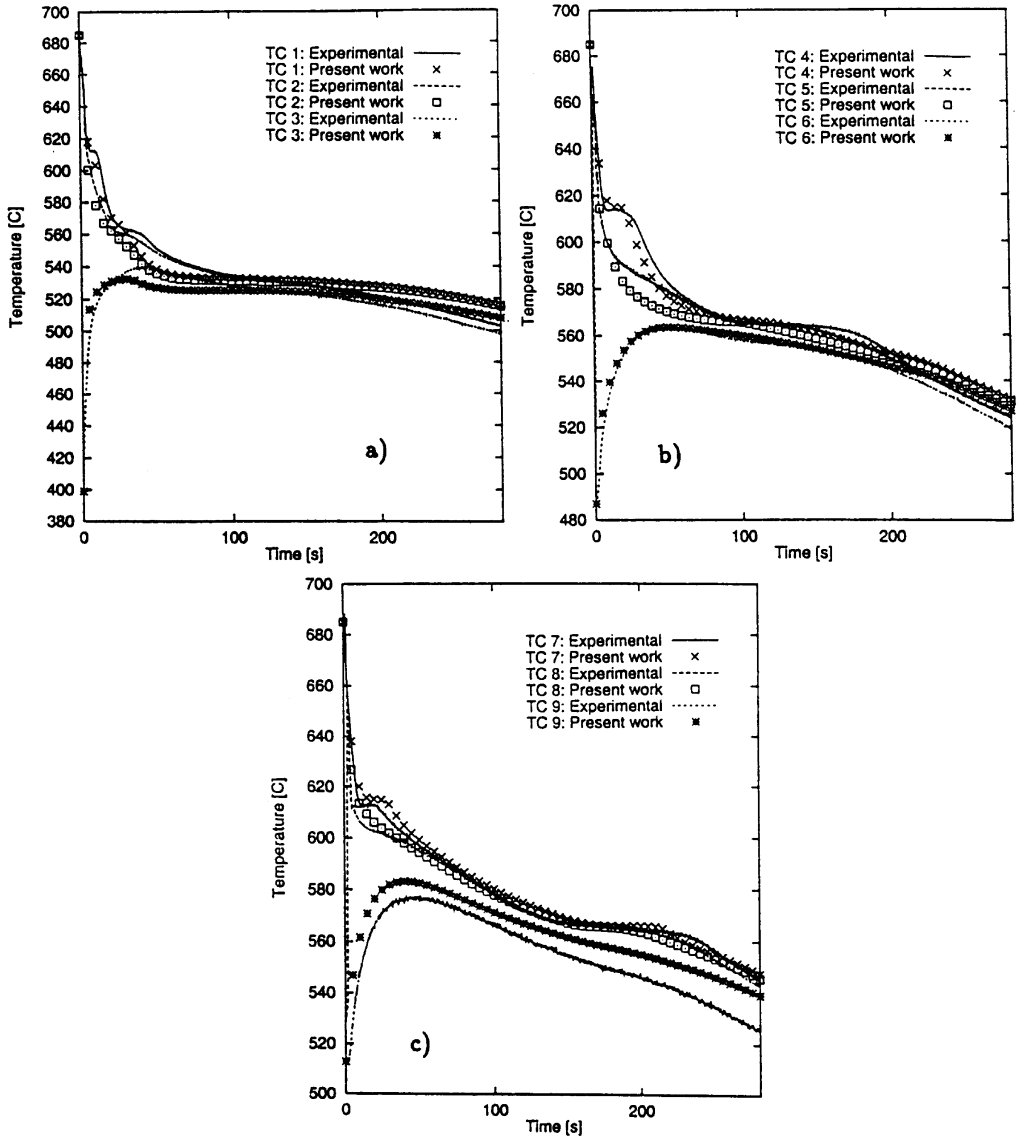

Fig. 6. Validation test: temperature evolutions for the experiment II: (a) thermocouples 1, 2 and 3, (b) thermocouples 4, 5 and 6 and (c) thermocouples 7, 8 and 9.

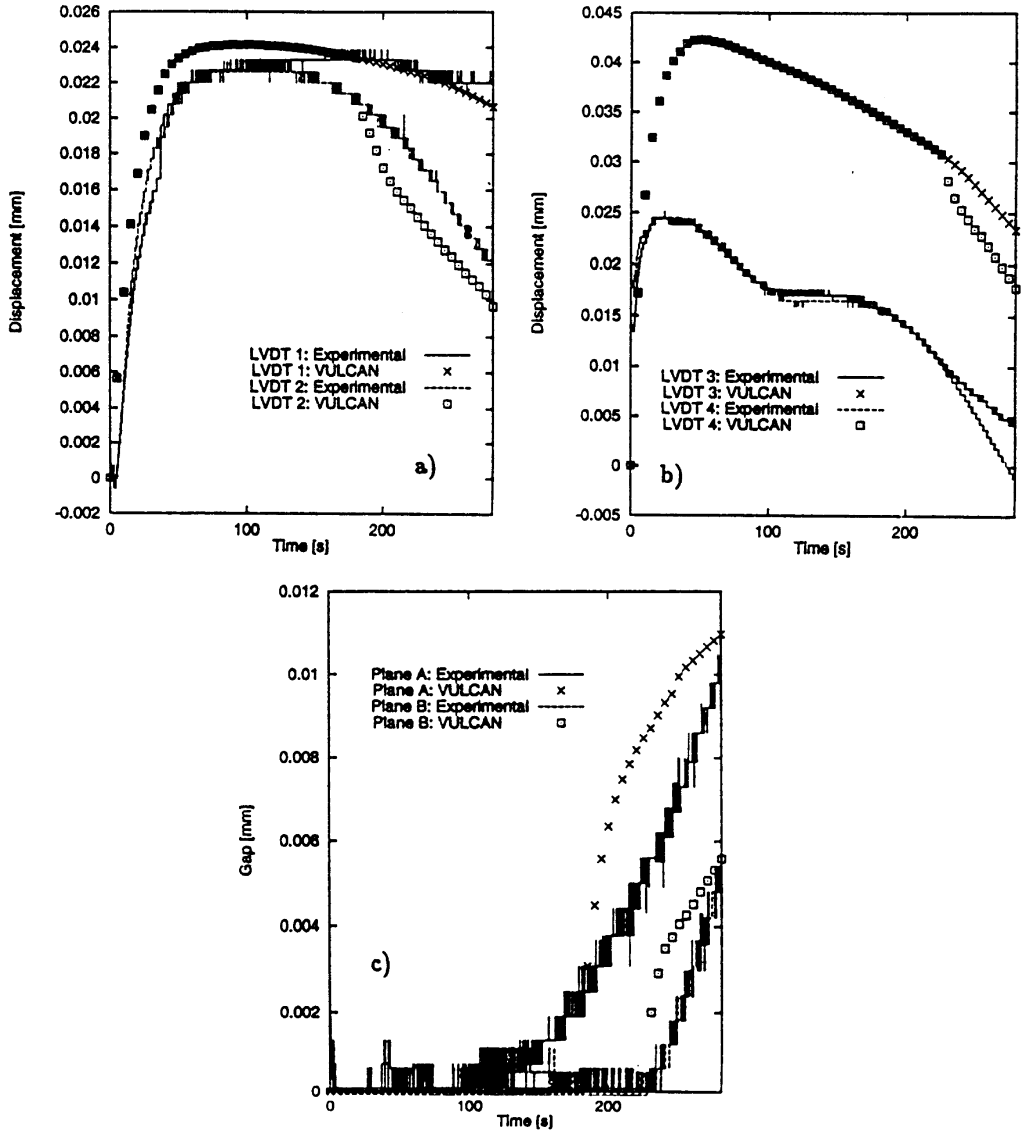

Fig. 7. Validation test: radial displacement evolutions for the experiment II: (a) LVDTs 1 and 2 and (b) LVDTs 3 and 4. Normal gap evolutions for the experiment II: (c) LVDT planes A and B.

References

Armero, F., Simo, J., 1992a. A new unconditionally stable fractional step method for non-linear coupled thermomechanical problems. International Journal for Numerical Methods in Engineering 35, 737–766.

Armero, F., Simo, J., 1992b. Product formula algorithms for nonlinear coupled thermoplasticity: formulation and nonlinear stability analysis. SUDAM Report No. 92-4, Stanford University.

Bellet, M., Ménaï, M., Bay, F., Schmidt, P., Svensson I., 1993. Finite element modelling of the cooling phase in casting processes. In: Piwonka, T.S., Voller, V., Katgerman, L. (Eds.), Proceedings of Modeling of Casting, Welding and Advanced Solidification Processes VI. The Minerals, Metals and Materials Society.

Bellet, M., Decultieux, F., Ménaï, M., Bay, F., Levaillant, C., Chenot, J., Schmidt, P., Svensson I., 1996. Thermomechanics of the cooling stage in casting processes: three-dimensional finite element analysis and experimental validation. Metallurgical and Materials Transactions B, Vol. 27B.

Cassenti, B., Annigeri, B., 1989. Thermodynamic constraints on stress rate formulations in constitutive models. Comput. Mech. 4, 429–432.

Celentano, D., 1994. Thermomechanical model for metal solidification problems (in Spanish). Ph.D. thesis, Universitat Politècnica de Catalunya (U.P.C.), Barcelona, Spain.

Celentano, D., 1996. VULCAN, thermal and coupled thermomechanical finite element analysis for solidification problems. User's Manual. Version 2.2.

Celentano, D., Pérez, E., 1996. A phase-change formulation including general latent heat effects. Int. J. Num. Meth. Heat Fluid Flow 6 (8), 71–79.

Celentano, D., Oller, S., Oñate, E., 1996. A coupled thermomechanical model for the solidification of cast metals. Int. J. of Solids and Structures 33 (5), 647–673.

Celentano, D., Oñate, E., Oller, S., 1994. A temperature-based formulation for finite element analysis of generalized phase-change problems. International Journal for Numerical Methods in Engineering 37, 3441–3465.

Celentano, D., Visconte, D., Dardati, P., Oller, S., Oñate, E., 1995. A thermomechanical model for solidification problems: experimental validation. In: Owen, R., Oñate, E., Hinton, E. (Eds.), Proceedings of Complas IV. Pineridge Press/CIMNE, pp. 2385–2396.

Chow, P., Bailey, M., Cross, M., Pericleous, K., 1995. Integrated numerical modelling of the complete casting process. In: Cross, M., Campbell, J. (Eds.), Proceedings of Modeling of Casting, Welding and Advanced Solidification Processes VII. TMS Publication, pp. 213–221.

Coleman, B., Gurtin, M., 1967. Thermodynamics with internal state variables. The Journal of Chemical Physics 47 (2), 597–613.

Flemings, M., Burke, J., Gorum, A., 1974. Solidification Technology. Butterworths, London.

Gunasegaram, D., van der Touw, J., Nguyen, T., 1995. Heat transfer at metal–mould interfaces. In: Proceedings of the IMMA/ADCA International Conference on Casting and Solidification of Light Alloys. Gold Coast, Australia, 30–31 August 1995, pp. 91–96.

Gunasegaram, D., Celentano, D., Nguyen, T., 1997. The effect of cooling a permanent composite mould on air gap formation and heat transfer. In: Proceedings of the Symposium on Application of Sensors and Modeling in Materials Processing, 126th TMS (The Minerals, Metals and Materials Society) Annual Meeting and Exhibition, Orlando, U.S.A., 9–13 February 1997.

Heinlein, M., Mukherjee, S., Richmond, O., 1986. A boundary element method analysis of temperature fields and stresses during solidification. Acta Mech. 59, 59–81.

Hughes, T., 1987. The Finite Element Method. Prentice-Hall International.

Kleiber, M., 1991. Computational coupled non-associative thermo-plasticity. Computer Methods in Applied Mechanics and Engineering 90, 943–967. North-Holland.

Lubliner, J., 1990. Plasticity Theory. Macmillan.

Nishida, Y., Droste, W., Engler, S., 1986. The air–gap formation process at the casting mould interface and the heat transfer mechanism through the gap. Metallurgical Transactions B 17B, 833–844.

Singer, A., Cotrelli, A., 1946. Properties of the aluminium–silicon alloys at temperatures in the region of the solidus. Journal of the Institute of Metals, pp. 33–54.

Smelser, R., Richmond, O., 1988. Constitutive model effects on stresses and deformations in a solidifying circular

cylinder. In: Giamei, A. F., Abbaschian, G. J. (Eds.), Modeling of Casting and Welding Processes IV. The Minerals, Metals and Materials Society.

Thévoz, P., Desbiolles, J., Rappaz, M., 1989. Modelling of equiaxed microstructure formation in casting. Metallurgical Transactions A 20A, 311–322.

Trovant, M., Argyropoulos, S., 1996. Mathematical modeling and experimental measurements of shrinkage in the casting of metals. Canadian Metallurgical Quarterly 35 (1), 75–84.

Vicente-Hernandez, P., Decultieux, F., Schmidt, P., Svensson, I., Levaillant, C., 1995. Mushy state behavior: rheological characterization and influence on air gap formation. ISIJ International 35 (6), 805–812.

Williams, J., Lewis, R., Morgan, K., 1990. An elasto-viscoplastic thermal stress model with applications to the continuous casting of metals. International Journal of Numerical Methods in Engineering 30, 579–599.

Wriggers, P., Miehe, C., 1992. Recent advances in the simulation of thermomechanical contact processes. In: Owen, R., Oñate, E., Hinton, E. (Eds.), Proceedings of Complas III. Pineridge Press/CIMNE, pp. 325–347.

Zabaras, N., Ruan, Y., Richmond, O., 1990. Front tracking thermomechanical model for hypoelastic–viscoplastic behavior in a solidifying body. Computer Methods in Applied Mechanics and Engineering 81, 333–364. North-Holland.

Zabaras, N., Ruan, Y., Richmond, O., 1983. On the calculation of deformations and stresses during axially symmetric solidification. Journal of Applied Mechanics 58, 865–871.

Ziegler, H., 1983. An Introduction of Thermomechanics. North-Holland.

Zienkiewicz, O., Taylor, R., 1989. The Finite Element Method. 4th edition, Vols 1 and 2. McGraw-Hill, London.